

Role of *BicDR* in bristle shaft construction and support of *BicD* functions

Aleksandra Jejina^{1,2}, Yeniffer Ayala³, Dirk Beuchle¹, Thomas Höhener¹, Ruth E. Dörig¹, Paula Vazquez-Pianzola¹, Greco Hernández³, and Beat Suter^{1,*}

¹Institute of Cell Biology, University of Bern, Switzerland

²Graduate School for Cellular and Biomedical Sciences, University of Bern, Switzerland

³Laboratory of Translation and Cancer, Unit of Biomedical Research on Cancer, Instituto Nacional de Cancerología (INCan), Mexico City, Mexico

*Correspondence: Beat.Suter@unibe.ch

Summary statement

Drosophila BicD and *BicDR* are needed for the elaboration of the F-actin bundles of macrochaetae and proper Rab6 and Spn-F expression. *BicDR* appears to support *BicD* in vesicle transport.

Running title: *BicD* and *BicDR* in bristle formation

Keywords: *Drosophila*, BicaudalD and BicaudalD-related, bristle formation, Rab6 and Spn-F, microtubule vesicle transport

Abstract

Cell polarization requires asymmetric localization of numerous mRNAs, proteins, and organelles. The movement of cargo towards the minus end of microtubules mostly depends on cytoplasmic dynein motors. In the dynein/dynactin/Bicaudal-D transport machinery, Bicaudal-D (*BicD*) links the cargo to the motor. Here we focus on the role of *Drosophila BicD-related* (*BicDR*) in the development of the long bristles. Together with *BicD*, it contributes to the

organization and stability of the actin cytoskeleton in the not-yet chitinized bristle shaft. *BicD* and *BicDR* also support the stable expression and distribution of Rab6 and Spn-F in the bristle shaft, including the distal tip localization of Spn-F, pointing to the role of microtubule-dependent vesicle trafficking for bristle construction. *BicDR* supports the function of *BicD* and we discuss the hypothesis whereby *BicDR* might transport cargo more locally and *BicD* over long distances, such as to the distal tip. We also identified embryonic proteins that interact with *BicDR* and appear to be *BicDR* cargo. For one of them, EF1 γ , we showed that EF1 γ genetically interacts with *BicD* and *BicDR* in the construction of the bristles.

Introduction

Microtubules are crucial for the growth of polarized cells. At the same time, they attach different cellular organelles, such as the nucleus, vesicles, the Golgi apparatus, and the endoplasmic reticulum, to a specific cellular compartment and enable the polarized transport of vesicles, mitochondria, mRNAs, and cytoskeletal elements (Bartolini and Gundersen, 2006; Bitan et al., 2010). Because of their growth, which is focused towards one pole of the cell (Bitan et al., 2010a), the *Drosophila* macrochaetae can serve as a model tissue for studying such cytoskeleton-dependent transport processes that are necessary for bristle development (Melkov et al., 2016). Several studies indicate that vesicle trafficking has an important function in this process (Rodriguez-Boulant et al., 2005). Multiple defects in bristle development have been described in flies that are mutant for members of the *Rab* gene family, which are known to regulate intracellular vesicle trafficking. Whereas *Rab6* and *Rab11* mutants eclose with short and stubble-like bristles, *Rab35* mutants display forks and kinks in their macrochaetae (Nagaraj and Adler, 2012; Purcell and Artavanis-Tsakonas, 1999; Zhang et al., 2009, 2007).

The *Drosophila* Bicaudal-D (*BicD*) is part of an evolutionarily conserved transport machinery, the microtubule-dependent dynein/dynactin transport apparatus. Its essential functions in the development of the oocyte and embryo are well characterized (Claußen and Suter, 2005; Schlager et al., 2010; Vazquez-Pianzola et al., 2022, 2014). Furthermore, it was observed that *BicD*^{A40V, S103A} and *BicD*^{null} mutants display short sternopleural and scutellar bristles (Koch et al., 2009). This mutant phenotype pointed to a function of *BicD* in the development of macrochaetae, one that had not been studied so far. The similarity between the bristle phenotype of *BicD* and *Rab6* suggested possible interactions between these two in constructing

the bristles. Support for this hypothesis comes also from work that showed that Rab6 and BicD function together in the delivery of secretory pathway components (Januschke et al., 2007).

The BicD protein family contains another member, BicD-related (BicDR, encoded by *CG32137*), which was discovered due to its strong sequence homology to BicD. In *Danio rerio*, BicDR is needed for the pericentrosomal transport of Rab6-positive vesicles during neural development. To perform this function, the *Danio rerio* BicDR requires the lysine residue K512, which is highly conserved between BicD and BicDR paralogues and orthologues (Schlager et al., 2010). The *Drosophila* BicD sequence around K730 is essential for the interaction with the cargo (Dienstbier et al., 2009) and a point mutation in this codon resulted in the isolation of the first single amino acid substitution that produced a *BicD^{null}* phenotype, indicating that this lysine is key to the physiological role of BicD (Ran et al., 1994). The homologous lysine in *Drosophila* BicDR is conserved and located at position K555 of BicDR-B and K461 of BicDR-A. For simplicity, we will refer to this residue as K555 for both isoforms. However, whether K555 of *Drosophila* BicDR serves the same function as its K730 orthologue of BicD remains to be tested. There are also interesting differences between BicD and BicDR. While *Drosophila* BicD consists of three coiled-coil domains, only the first and third are conserved in the BicDR protein.

Although the strong homology between the fly BicD and BicDR suggests similar functions, the role of *BicDR* in *Drosophila* has not yet been examined. The homology is strongest in the coiled-coil domain near the C-terminus which, in the case of BicD, is known to be needed for the attachment and transport of various cargoes (Dienstbier et al., 2009; Schlager et al., 2010).

We set out to investigate the function of *BicDR* with a focus on a potential role in MT-dependent trafficking and possible cooperation or competition between BicDR and BicD that might contribute to the development and maintenance of polarized cell growth. Here we describe the genetic interaction between *BicD* and *BicDR* and its contribution to fly development. Furthermore, we describe and compare the effect of different *BicD* and *BicDR* alleles on the formation of the macrochaetae.

Results

Functional redundancy between *BicDR* and *BicD*

While BicD consists of three coiled-coil domains, only the first and third are conserved in the related BicDR protein (Fig. S1A). The homology is strongest in the coiled-coil domain near the

C-terminus, which in the case of BicD is known to be needed for the transport of different cargoes (Dienstbier et al., 2009; Schlager et al., 2010). Although the N-terminus is less highly conserved between the two proteins, it was shown that BicD and BicDR require it for the efficient binding to dynein and dynactin *in vitro* (Splinter et al., 2012); (Urnavicius et al., 2018).

Drosophila BicDR extends over 24.4 kb of genomic sequence with 6-8 exons in total (Fig. S1B). Remarkable is the relatively long intron with about 18 kb between the first and second protein-coding exons, which is also similar to the structure of the *BicD* gene (Thurmond et al., 2019). There are two transcripts: *BicDR-A* and *BicDR-B* with the difference that the *BicDR-A* start codon is localized 282 bp downstream of the *BicDR-B* one. Both transcripts share the reading frame and the stop codon. The extra peptide of BicDR-B contains a repeat of 5 Asparagine and 6 Serine residues, respectively, but shows no homology to any other gene or organism.

To identify specific *BicDR* alleles that could be null alleles, we picked two P-element insertions and created imprecise excision mutations (see Methods section). For further genetic analyses, we retained two excision lines from the upstream element and one from the downstream insert: *BicDR*²⁹, *BicDR*⁵¹, and *BicDR*⁷¹ (Fig. S1B). While the excision *BicDR*²⁹ removed only the 5' UTR region, excision *BicDR*⁵¹ removed in addition to that also the entire first protein-coding exon. *BicDR*⁷¹ is the only excision that removes the second, third, and fourth protein-coding exon and thereby also induces a stop codon in the first coiled-coil domain of BicDR-A and BicDR-B (Fig. S1). In addition, we retained a precise excision *BicDR*^(rev) from the downstream element as a control. We also generated a precise mutation where the Q554 and K555 codons in *BicDR* were deleted (*BicDR*^{8.1}, see Fig. S1B).

All the described *BicDR* mutants were viable and fertile, indicating that *BicDR* is a non-essential gene. However, hemizygous *BicDR*⁷¹ females eclosed with individual macrochaetae that contained discolored and brittle tips that bent or broke off easily (Fig. 1; white arrow pointing to a white bristle tip in Fig. 1C). Additionally, a fraction of the female adults contained additional aSC, aPA, or pNP macrochaetae (Takano, 1998) (see white arrows pointing to shorter pSCs and a blue arrow to an additional aSC in Fig. 1D). This phenotype was not observed in *BicDR*²⁹ mutants. Knocking down *BicDR* by RNAi driven with the *en-Gal4* driver also led to adult females eclosing with individual slightly shorter aSC or pSC macrochaetae (Fig. 1E). This phenotype could be observed significantly more often in females than in males. 12 out of 18 female and 2 out of 8 male flies eclosed with at least one shorter bristle, while no control animals (0 out of 32 *en-Gal4; UAS-GFP*) displayed such a phenotype (Fig. 1F). These results show that *BicDR*

functions in the formation and development of mechanosensory organs of *Drosophila* during metamorphosis.

The sequence similarity between BicD and BicDR suggests that the two proteins might either be functionally redundant or compete with one another. To test these possibilities, we produced flies that simultaneously carry mutations in both genes using a female sterile allele of *BicD* (*BicD^{PA66}*) (Schüpbach and Wieschaus, 1991; Suter and Steward, 1991). *BicD*; *BicDR* double mutants of the genotype *BicD^{PA66}/-*; *BicDR^{*}/-* were tested for viability and fertility. *BicDR^{*}* stands for the different *BicDR* alleles tested (*BicDR²⁹*, *BicDR⁵¹*, *BicDR⁷¹*, and *BicDR^{8.1}*) and the wild-type revertant *BicD^(rev)* that served as a control.

As shown in Fig. 2A, hemizygous double mutant males and females were virtually absent from the offspring but appeared in the control *BicD^{PA66}/-*; *BicDR^(rev)/-* (13% of the total number of eclosed progeny, which is the expected frequency for the control). The genotype *BicD^{PA66}/-*; *BicDR⁷¹/-* was only found in three male flies (0.65% of all eclosed progeny; Fig. 2A). No progeny of the genotypes *BicD^{PA66}/-*; *BicDR⁵¹/-* and *BicD^{PA66}/-*; *BicDR^{Df}/-* or *BicD^{PA66}/-*; *BicDR^{8.1}/-* eclosed, while 21 animals with the genotype *BicD^{PA66}/-*; *BicDR²⁹/-* eclosed (5.37% of the total eclosed progeny). The genotype *BicD^{PA66}/-* is viable, but if both copies of *BicDR* are additionally null or strong loss-of-function alleles, the flies are not viable anymore. We conclude that one functional copy of *BicDR* is sufficient to support the residual *BicD* function in *BicD^{PA66}/-* and maintain viability. This points to a redundant role of *BicD* and *BicDR* for an essential function.

The few *BicD^{null}* animals that survived to adulthood displayed a bristle defect phenotype with colorless and brittle bristle tips (Koch et al., 2009). Whereas the discolored tips were already seen in *BicD^{PA66}/-* flies (Fig. 2B), much shorter bristles only appeared when *BicDR* activity was also reduced in this background (*BicD^{PA66}/-*; *BicDR^{*}/+*). These animals eclosed with significantly shorter, stubble-like macrochaetae (Fig. 2B). This short bristle phenotype was the strongest in flies that carried the *BicDR⁷¹* and *BicDR^{8.1}* allele: all adult progeny with a hemizygous copy of *BicD^{PA66}* and one *BicDR⁷¹* (or *8.1*)/+ chromosome showed the short bristle phenotype (Fig. 2C). The same was true when the *BicDR* deficiency chromosome (*BicDR^{Df}*) was tested in the same way (*BicD^{PA66}/-*; *BicDR^{Df}/+*). In contrast, less than half of the hemizygous *BicD^{PA66}* flies containing *BicDR⁵¹* and *BicDR²⁹* eclosed with short bristles. For *BicDR²⁹*, these were 35% (8 out of 23 flies), and for *BicDR⁵¹* 33% (5 out of 15 flies). These results show again that *BicDR⁺* supports *BicD^{PA66}* in bristle development but only a single functional copy of *BicDR* is not sufficient to allow normal bristle development.

The genetic analyses of the mutant *BicDR* alleles define an allelic series. The *BicDR*²⁹ is a hypomorphic allele and produces the weakest phenotype because hemizygous *BicD*^{PA66} animals that are also hemizygous for *BicDR*²⁹ are viable, whilst the analogous genotype is lethal for *BicDR*⁷¹, *BicDR*⁵¹, or *BicDR*^{Df}. *BicDR*²⁹ seems to retain considerable functional *BicDR* activity, and this seems possible because the excision only removed the 5' UTR region and intron sequences of *BicDR* but no protein-coding regions (Fig. S1). On the other hand, the *BicDR*⁷¹ allele is the strongest. Our results reveal that the allele *BicDR*⁷¹ induces the strongest effect within flies that contain the hypomorphic mutation *BicD*^{PA66}. We can further conclude that *BicDR*⁷¹ is a stronger *BicDR* allele than *BicDR*⁵¹ and that its behavior can be compared to the deficiency of *BicDR*, *BicDR*^{Df}, which removes the *BicDR* gene completely. *BicDR*⁷¹ removes protein-coding exons 2 and 3, while *BicDR*⁵¹ removes the 5' UTR region and the first protein-coding exon of *BicDR*-A and -B (Fig. S1). The independently generated allele *BicDR*^{8.1} (= *BicDR*^{ΔGK555}) also appeared to be a null allele like *BicDR*⁷¹ but was not tested as much as the latter.

A more detailed picture of the different bristle phenotypes was obtained with the scanning electron microscope (SEM; Fig. 2D-H; Fig. S2). The average length of unbroken pSC bristles was around 455μm for the wild type (Fig. 2D). The *BicDR*^{-/-} pSCs reached 82% of this length (Fig. 2E; the average of the measured length was 375μm) and the *BicD*^{*}/+; *BicDR*^{-/-} pSCs reached 70% of the normal size (Fig. 2F; 320μm; *BicD*^{*} stands for *BicD*^{PA66} or the *BicD* deficiency). *BicD*^{PA66}/+ pSCs reached 78% of the normal size (Fig. 2G; 355 μm) and additional inactivation of one copy of *BicDR* brought this down to only 35% of the normal size (Fig. 2H; 160μm). Bristles contain actin filament bundles which are known to shape the cuticle ridges seen on the surface of the adult bristles. These ridges are prominently seen in the proximal region close to the base where they are separated by deep grooves (Fig. 2D). In the wild-type bristles, these ridges (and presumably also the underlying actin bundles that shape them) are amazingly straight all the way to the region of the tip and only a few ridges seem to merge. In apparently full-length *BicDR* bristles, the ridges are also seen in the tip, but the tips often appear frayed with individual ridges or small groups of ridges separating from others, dissolving the tip into several small tips (Fig. S2). This suggests that the underlying actin bundles are less glued together and less straight. In the *BicD*^{PA66}/+ situation, the ridges are straight in most parts of the bristle, but the grooves, which seem to form normally close to the base, become less prominent in the more distal regions. In the still conical tip, the ridges with the bundle structure appear less straight and more twisted or braided. This phenotype becomes strongly enhanced by removing

one copy of *BicDR*. In the *BicD^{PA66}/-*; *BicDR*^{+/+} background, the ridges with their bundle structure are apparent only very close to the base and get lost on the surface in the more distal region (see also Fig. 2H). This phenotype closely resembles a *rab6/warhog* phenotype described by Purcell and Artavanis-Tsakonas (Fig. 2d in Ref⁹). In this background, we observed frequently broken bristles with a large diameter in proximal bristle regions (Fig. S2).

In the *BicDR* mutants, we observed very thin and flattened bristles in the more distal regions and many displayed kinks and frayed tips. If these mutants have only one *BicD*⁺ copy, the tips appear more twisted and braided (Fig. S2).

Lack of *BicDR* function also led to a slightly reduced bristle thickness in the proximal region just above the bristle base (9-10µm compared to slightly over 10µm; overview pictures in Fig. S2). Surprisingly, the phenotype of the *BicD^{PA66}/-* bristles differed from the wild-type in the opposite direction. These bristles were between 11-13µm thick in the corresponding proximal region.

One mechanism by which *BicDR* might support *BicD* function is suggested by their similar structure. *BicD* functions as a dimer, which it forms through its coiled-coil domains. If the homologous coiled-coil domains interact, *BicDR* might replace a *BicD* subunit in the active complex. To test whether *BicD* and *BicDR* form heterodimers we tested for this interaction in a yeast two-hybrid experiment, which would reveal direct interactions between the two proteins. The yeast two-hybrid experiment confirmed that *BicDR* forms homodimers (Fig. S3), as had been already described (Chaaban and Carter, 2022; Urnavicius et al., 2018). However, the experiment did not reveal any direct interaction between *BicD* and *BicDR*. Similarly, immunoprecipitations with embryos expressing GFP-tagged *BicDR* did not reveal copurification of the two related proteins by Western blotting or MS analysis (see below). Therefore, our results did not provide evidence that *BicDR* supports *BicD* function by forming dimers.

***BicDR::GFP* is expressed in the salivary glands and the embryo in a metameric pattern**

To determine in what tissues and during which embryonic stages *BicDR* is expressed, we tagged the *BicDR* gene endogenously with GFP using CRISPR/Cas9 and immunolocalized *BicDR::GFP* in embryos after fixation. This method allows us to track both translated *BicDR*-A and *BicDR*-B. Through sequencing, we confirmed that the *BicDR* ORF was fused seamlessly with the eGFP ORF. The successful ORF fusion and the expression of the predicted fusion protein were also confirmed by Western blotting of embryonic extracts which revealed the GFP expression as part of a 120 kDa polypeptide (Fig. 3A).

Immunolocalization of BicDR::GFP in embryos revealed that the apical side of salivary gland cells stained very strongly from stage 13 on (white arrow in Fig. 3B, higher magnification shown underneath). Additionally, individual cells displayed staining signals in a metameric manner along the lateral side of the embryo. These signals were most intense during stages 11-14 (Fig. 3C, top). By co-immunostaining of the cytoplasmic BicDR::GFP and the nuclear neuroblast marker Asense (Ase), which is expressed in all sensory organ precursor (SOP) cells and their progeny (Berdnik et al., 2002), cells with the strongest BicDR::GFP signal are seen in the region of Ase positive cells. Whereas some stronger signals seem to overlap, often the two different signal peaks appear to be rather in adjacent cells (Fig. 3C). Because initial experiments did not reveal a function of *BicDR* in salivary glands but identified defects in the adult bristles of the mutants, we focused on the function of *BicDR* in bristle development.

***BicD* and *BicDR* contribute to localizing Rab6 to the tip of the mechanosensory bristles**

To further understand bristle development and the impact of *BicD* and *BicDR* on it, pupal dorsal tissue containing the developing bristles was dissected 40 to 44 hours after pupation, fixed, and stained. In this way, hemizygous *BicD*^{PA66} samples with only one functional copy of *BicDR* were compared to *BicD*^{PA66} animals with two functional *BicDR* copies and to controls that were wild-type for *BicD* and *BicDR*. Investigating the F-actin structure of the samples allowed us to compare the length and morphology of the macrochaetae (Fig. 4A,B). Comparing the pupal bristle length in the mutants with the wild type showed that the mutant bristles appeared somewhat shorter but that there were no significant length differences (Fig. 4A). This indicates that the short bristle phenotype observed in *BicD*; *BicDR* double mutant flies evolved at a later stage of development. Although similar in length, the actin cytoskeleton of the double mutant scutellar bristles displayed abnormalities. 6 out of 7 mutant scutellar macrochaetae showed an irregular arrangement of the actin bundles, and obvious gaps could be observed (Fig. 4B). This phenotype could not be observed in the control pupae (0 out of 4 scutellar macrochaetae) nor in hemizygous *BicD*^{PA66} animals. While such gaps in the actin bundles are reminiscent of the chitinization process of the bristles, this does not appear to be the reason because all pupae were only 40 to 44 hours into pupation. The breakdown of the bundles by chitinization, however, begins only 48 hours after pupation and it shows initially narrow longitudinal gaps between modules, and these become wider as the bristle ages. Only in 53 hours old pupae such breakdown becomes clearly recognizable (Tilney et al., 1996).

Rab6 is known to be a Notch modifier that influences the development of the mechanosensory bristles on the head, notum, and scutellum. The *Rab6* phenotype also results in aberrant bristle length and bristle tips that have very mild and disorganized ruffling (Purcell and Artavanis-Tsakonas, 1999). This phenotype resembles the short bristle phenotype observed in *BicD*; *BicDR* double mutants. Additionally, Schlager and colleagues described a physical interaction between Rab6 and BicDR in *Danio rerio* (Schlager et al., 2010), and Januschke et al. an interaction between *Drosophila* Rab6 and BicD (Januschke et al., 2007). We, therefore, examined the *Rab6* distribution in the macrochaetae of *BicD^{PA66}/-* and *BicD^{PA66}/-; BicDR^{+/+}* mutants. For this, we stained the pupal dorsal tissue for Rab6. As seen in Fig. 4C,D, and Fig. S4, in the wild-type scutellar bristle the Rab6 signal is present along the entire shaft, but there appears to be a higher Rab6 level at the proximal end and a gradual reduction towards distal, often followed by a second, smaller peak at the tip. For Figs 4D and S4, channel signal intensities were normalized per channel, allowing a better impression of the signal distribution in the bristle. Fig. S5 shows the same primary data normalized across all three channels. This allows one to detect changes in signal levels from genotype to genotype if the experimental conditions are the same and the background signals are low. In the wild type, the Rab6 signal was similarly strong as the F-actin signal. In the *BicD* mutants and particularly in the double mutants Rab6 levels were drastically reduced compared to the F-actin signal and only weakly seen in parts of the bristle (Fig. S5), revealing that Rab6 expression levels strongly depend on functional *BicD* and *BicDR*. In *BicD^{PA66}/-; BicDR/-* mutants, residual Rab6 signal appears evenly distributed throughout the bristle shaft without a discernable distal tip accumulation.

***BicDR* and *BicD^{PA66}* in localizing Spn-F to bristle tips**

Spindle-F (Spn-F) is a microtubule minus-end marker that affects oocyte patterning and bristle morphology in *Drosophila* (Abdu et al., 2006). *Spn-F* mutants eclose with shorter and thicker bristles. Scanning electron micrographs of the bristles revealed that the mutant bristles have branching tips and that the direction of elongation is sometimes perturbed (Abdu et al., 2006). Spn-F functions at the distal tip of the growing bristle and is involved in the regulation of the shuttling movement of recycling endosomes and cytoskeletal organization (Otani et al., 2015). We analyzed the potential requirement for *BicD* and *BicDR* for the localization of Spn-F to and within the shaft of the bristle cells (Figs 4C, 5, S4, S5). The normal asymmetric localization to the tip of the macrochaetae allowed us to assess the contribution of *BicD* and *BicDR* to this microtubule minus-end transport process. One measure for the establishment of the polarity of

the bristles is the “tip index”: a line scan from the bristle shaft to the distal tip establishes a plot profile from which the maximum intensity along the bristle length is determined. The “tip index” is defined as the relative position of the pixels that exceed 50% intensity along the bristle axis (Otani et al., 2015). This index is used to quantify the asymmetric localization of a protein within the bristle cell. If a signal is completely localized at the bristle tip, the tip index will have a value of 100. If the signal remains in the cell body and stays absent from the bristle, the value of the tip index is 0 (Otani et al., 2015). This measurement confirmed that the Spn-F signal is significantly more concentrated at the tip of the macrochaetae of control pupae, while this signal tends to appear diffusely throughout the whole cell in *BicD^{PA66}/-* and *BicD^{PA66}/-; BicDR⁷¹ / +* bristles (Fig. 5A,B). The tip index in control macrochaetae had a value of 33, while the value in *BicD^{PA66}/-; BicDR⁷¹/+* bristles was 18. Similar to this, the tip index in *BicD^{PA66}/-* bristles was 16. These results suggest that *BicD* is necessary for the localization of Spn-F to the distal tip.

Similar to the reduction of Rab6, the Spn-F signal in the pupal bristle is also strongly reduced, particularly in the *BicD^{PA66}/-; BicDR⁷¹/+* double mutants (Fig. S5). Additionally, the Spn-F signal ratio in the bristle shaft versus cell body changes between *BicD^{PA66}/-* and *BicD^{PA66}/-; BicDR⁷¹/+* double mutants (Fig. 5C). To quantify this, we measured the average signal strength of an area on a plane in the center of the bristle shaft and divided this by the average signal strength of an area of the same size drawn on a plane through the bristle cell body, directly under the bristle root. While *BicD^{PA66}/-* bristles show a wider distribution of this ratio, the ratio decreases significantly in *BicD^{PA66}/-; BicDR⁷¹/+* bristles in comparison to the wild type. One might, for instance, expect to find such a distribution if BicDR is more involved in localizing Spn-F to the periphery of the macrochaetal cell body and BicD more for the long-range transport along the bristle shaft towards the bristle tip.

At the developmental stage when we observed these localization differences, the length of the mutant macrochaetae was not significantly reduced yet (Fig. 4A). It thus appears that strongly reduced Rab6 and Spn-F levels in combination with a defective actin cytoskeleton might prevent normal bristle construction in *BicD^{PA66}/-; BicDR⁷¹/+* mutants. The reduced distal tip localization of Spn-F and Rab6 might be an additional factor contributing to the bristle phenotype.

EF1 γ is found in BicDR complexes and EF1 γ enhances the bristle phenotypes of *BicD* and *BicdR*

To learn more about the mechanisms through which BicDR contributes to transport processes in general, we used the C-terminally tagged endogenous *BicDR* (*BicDR::GFP*), which displays a wild-type bristle phenotype, and performed immunoprecipitations with an anti-GFP antibody using extracts from 10-16 hours old embryos. We also mutated the endogenous gene into a *BicDR*^{K555A}::*GFP* gene and used it as a control because it might allow us to distinguish between the cargo that binds through the K555 region and other interacting partners of BicDR. A *white*⁻ strain with an untagged *BicDR*⁺ was used as another negative control. The search for interacting proteins was performed in 2 different ways. First, in triplicate experiments, embryos were lysed and immunoprecipitated with anti-GFP antibodies. A proteomic analysis was then performed directly on the precipitated fractions. Second, embryos were lysed in duplicates, immunoprecipitated as before, and the resulting proteins were separated by SDS-PAGE. The gel was stained by Coomassie blue and only those bands found in the tagged *BicDR::GFP* fraction and not in the *BicDR*^{K555A}::*GFP* samples were excised and analyzed. Gel slices from the corresponding position of the control samples were also analyzed.

The results of the first IP experiment defined 25 potential *BicDR::GFP* interactors with a p-value ≤ 0.05 and $\log_2FC \geq 1.0$ (Supplementary data file S1). Of these, 7 were also found in *BicDR*^{K555A}::*GFP* samples, indicating that these are binding partners that depend less on K555. Out of the remaining 18 candidates, different bristle phenotypes had already been described for 4 mutants (*tou*, *RpS17*, *RpL27A*, and *RpL12*) (Casad et al., 2011; Hart et al., 1993; Vanolst et al., 2005) while RNA binding activity had been observed for *RpS5b* (Kong et al., 2019) (Table S1). Whereas ribosomal proteins are a common contaminant in IPs, mutations in ribosomal protein genes lead to impaired bristle development and show a haploinsufficiency phenotype that is seen as evidence for a very high protein synthesis required for bristle development (Marygold et al., 2007). It is therefore also possible that BicDR interacts with ribosomes. *Tou*, on the other hand, is a transcription factor that activates proneural gene expression (Vanolst et al., 2005) and has also been found in a gain-of-function screen for genes that affect external sensory organs (Abdelilah-Seyfried et al., 2000). The overexpression of different *tou* alleles results in excess scutellar and dorsocentral macrochaetae (Abdelilah-Seyfried et al., 2000; Peña-Rangel et al., 2002).

Other noteworthy candidates identified in this IP are *Rac1* and *morpheus* (*mey*). Although identified with only a few counts, *Rac1* is significantly enriched in the IP with the wild-type

BicDR::GFP peptide. Rac1 has been associated with axial outgrowth (Bagley et al., 2014; Leiss et al., 2009), control of lumen size of salivary glands (Jenkins et al., 2022), and activities in tracheae, embryonic salivary glands (Chihara et al., 2003; Pirraglia et al., 2006), and bristles (see FlyBase; (Jenkins et al., 2022)), where overexpressing of a mutant *Rac1* allele causes defects. Rac1 is therefore interesting for further analysis of the *BicDR* function.

In the second approach with gel-purified bands, the larger sample size yielded 179 interacting proteins in the tagged wild-type BicDR::GFP IP that were not present in the IP of the tagged BicDR^{K555A}::GFP mutant protein (Fig. 6A; Supplementary data file S2). Because the *BicDR*⁷¹ chromosome showed a bristle duplication indicative of a problem in Notch-dependent binary cell fate acquisition (Le Bras et al., 2012), and because Notch signaling also depends heavily on cytoplasmic transport, we searched among the proteins identified in the BicDR::GFP IP for known trafficking regulators of the Notch receptor (Table S2). Origin recognition complex subunit 6, Vacuolar H⁺ ATPase subunit 68-2, Vacuolar H⁺ ATPase 26kD E subunit, Rumi, Par-6, and Ef1γ are all Notch-trafficking regulators that were absent in the control IPs but detected in the BicDR::GFP IPs. Except for *par-6*, loss-of-function mutations of all the genes for these candidate interactors result in bristle loss (Le Bras et al., 2012).

The translational regulator Ef1γ appeared particularly interesting because its mutants display a bristle phenotype, and it was immunoprecipitated at the highest amount among the identified potential binding partners of BicDR. Aside from its function in translation, EF1γ is known to negatively regulate the transport of several classes of membrane organelles along microtubules (Serpinskaya et al., 2014) and for its interaction with keratin bundles in mouse fibroblasts (Kim et al., 2007). For these reasons, we further investigated the interaction with *EF1γ*. To test whether the two genes might act in the same pathway, we first compared their mutant phenotypes (Fig. 6B-H). While the alleles *EF1γ*^{A42} and *EF1γ*^{A28} induced additional aSC macrochaetae at either only one or both sides of the notum (Fig. 6F,G), the mutants *EF1γ*^{A70} and *EF1γ*^{A15} eclosed with shorter pSC macrochaetae, similarly to hemizygous *BicDR*⁷¹ flies (compare Fig. 6E,H and Fig. 6D).

Flies transheterozygous for *BicDR*⁷¹ and *EF1γ* are viable and 2-13% of them displayed shorter pSC or aSC macrochaetae (*BicDR*⁷¹ and *EF1γ*^{A28}: 2%; *BicDR*⁷¹/*EF1γ*^{A15}: 5%; *BicDR*⁷¹/*EF1γ*^{A70}: 13%; Fig. 6I-K). This effect could not be observed in *BicDR*^(rev) / *EF1γ*^{A28} mutants or heterozygous *EF1γ*^{A28} animals. The phenotype was significantly more prominent if the flies were transheterozygous for *BicD*^{PA66} and *EF1γ*^{A28}: 23% of the animals showed at least one shorter

bristle. This went up to 48% with *BicD*^{PA66} / +; *EF1γ*^{A70} / +, whereas in *BicD*^{PA66} / +; *EF1γ*^{A15} / + flies 17%; showed at least one short bristle (Fig. 6I-K). To test if a mutant *BicDR* allele enhances the phenotype of transheterozygous *BicD*^{PA66}; *EF1γ*^{A28} mutants even further, we generated flies that were heterozygous for all three genes. 44% of all *BicD*^{PA66} / +; *BicDR*⁷¹ / *EF1γ*^{A28} eclosed with at least one shorter bristle (26% in *BicD*^{PA66} / +; *BicDR*⁷¹ / *EF1γ*^{A15} animals and 30% in *BicD*^{PA66} / +; *BicDR*⁷¹ / *EF1γ*^{A70}).

In summary, we conclude that except for allele *EF1γ*^{A70}, the proportion of animals with shorter bristles is significantly higher if they are heterozygous for all three mutants, *BicD*^{PA66}, *BicDR*⁷¹, and *EF1γ*, indicating that all three genes are functioning in the same direction and contribute to proper macrochaetae development. This appears surprising because BicD and BicDR help to perform MT transport whereas *EF1γ* negatively regulates it. The observed type of genetic interaction can be explained if *EF1γ* performs its function at the bristle tip and negatively regulates organelle transport there, allowing the organelles to perform their function at the tip. Unfortunately, the antibody localization of EF1γ did not allow us to test the distribution of EF1γ in the pupal bristles. Presumably because of the high signal levels in all tissues, one would need to use a more complex approach to test whether EF1γ can be linked more closely to *BicD* and *BicDR* activity.

Also in this situation, the female flies were much more affected by this phenotype than the males and additional bristles could be observed at low frequency in the mutants *BicD*^{PA66} / +; *BicDR*⁷¹ / *EF1γ*, but also in the controls (*EF1γ* / + and *EF1γ* / *BicDR*^(rev)). The similar bristle phenotype, the genetic interaction between *EF1γ* and *BicDR*, and the fact that BicDR::GFP and EF1γ co-precipitated posed the question of whether they interact directly. However, a yeast two-hybrid assay did not detect a direct interaction between BicD, BicDR, or EF1γ (Fig. S3).

Because EF1γ was the top hit in this group and the genetic interaction assay testing for combined haploinsufficiency showed strong interactions with the *EF1γ* alleles (Fig. 6), we focused on *EF1γ* for the proof of principle in the present study. Interesting additional interactors from the same screen are Arp2 and Arp3 (Table 2). The Arp2/Arp3 complex is involved in the organization of the actin filaments, a structure that is affected by the reduced *BicD*; *BicDR* function (Fig. 4).

Discussion

We found that *BicDR* is not an essential gene, but it has important functions in the development of the long bristles, the macrochaetae (Figs 1, 2). Additionally, one functional *BicDR* copy is essential for viability in a hypomorphic *BicD* background. In these animals with reduced *BicD* activity and only one functional copy of *BicDR*, the remaining combined activities of *BicD* and *BicDR* are not sufficient to develop bristles properly (Fig. 2). Here we showed that the reduced activity of *BicD* and *BicDR* affects the Rab6 and Spn-F levels and localization in the growing bristle, linking *BicD* and *BicDR* to the dynein-dependent microtubule transport of vesicles and bristle factors to their proper position in the bristle where they perform their function.

A different defect in the development of the bristle, the formation of a twin bristle on the notum, was seen in 21% of hemizygous *BicDR*⁷¹ flies (Fig. 1D). This was mostly an additional aSc bristle with a hair and socket of its own. This hinted at a failed cell fate acquisition after the division of pl cells that can result from gain-of-Notch signaling in the cell divisions leading to the sensory organ formation (Le Bras et al., 2012). This connection was also attractive because the Notch trafficking regulator EF1 γ (Le Bras et al., 2012) was a top hit for *BicDR* interacting proteins and transheterozygous *EF1 γ /*BicDR*^{Df}* also showed bristle duplications. *BicDR*^{Df} lacks, aside from *BicDR*, 8 other genes. However, the evaluation of the cause of this phenotype became too challenging for now because animals in the control group *BicDR*^(rev)/-, a wild-type revertant generated by hopping out the P-element insertion that was used to generate the *BicDR*⁷¹ allele through an imprecise excision, also showed twin bristles in 7% of the animals. On the other hand, excision mutants and revertants that were generated with the P-element that had inserted in the 5' region of *BicDR* (Fig. S1) did not show this phenotype. A possible interpretation might be that the P-element chromosome had acquired a second hit that supports bristle duplications. Such second-site hits are common and often caused by local transpositions, which would explain why the *BicDR*^{Df} chromosome also showed this interaction with EF1 γ (Fig. 6I-K). Because of the difficulty of resolving this issue, we focused on the bristle growth phenotype to gain more insights into the function of *BicDR*.

The second coiled coil domain of *BicD* ensures that the adaptor protein remains inactive if no cargo is bound. For this, the cargo-binding, third coiled coil domain folds back onto the second coiled coil, thereby blocking the dynein interaction site (reviewed by Suter, 2018). This mechanism ensures that the *BicD*-transport machinery does not run unloaded along microtubules. *BicDR* lacks this second coiled coil domain, suggesting that *BicDR* itself does not have an activated or inactivated state or controls this through a different mechanism. A second

dissimilarity between *BicD* and *BicDR* is the big difference between their expression levels. According to Flybase (Jenkins et al., 2022), *BicDR* is mainly expressed in tracheae, gut, salivary glands, and carcass tissue, while the expression in other tissues remains at low levels. Although there is some overlap with the expression of *BicD*, the expression of *BicDR* was described to remain low in the tissues where the consequences of *BicD* mutations have been described. Such tissues are the ovary, the young embryo, and the nervous system (Aradska et al., 2015; Sanghavi et al., 2016; Vazquez-Pianzola et al., 2011). This allows the assumption that the expression of *BicDR* at low levels does not necessarily contribute to cargo transport the same way as *BicD* does. How could *BicDR* then support *BicD*? It does not appear to dimerize with a *BicD* subunit based on immunopurification or yeast 2-hybrid results (Fig. S3, Tables S3, S4). *BicD* is more important in large cells where it transports cargo over very long distances. *BicDR* might be specialized for moving cargo for local transport over short distances (e.g., from the cell body into the bristle shaft). In cells where both are expressed, *BicDR* may then make the cargo more accessible for long-distance transport by *BicD*. This seems consistent with the function we found in the growing bristle shaft, where *BicDR* seems more involved in bringing Spn-F from the cell body to the shaft and *BicD* to transport it toward the tip (Fig. 4). While the proper tip localization of Spn-F depends on *BicD* and *BicDR*, we found that in the sensitized background (*BicD*^{PA66}/-) both copies of *BicDR* are needed to move normal levels of Spn-F from the cell body into the bristle shaft (Fig. 5C). On the other hand, full *BicD* activity is not required for this step (Fig. 5C) but is required to obtain strong bristle tip localization of Spn-F (Fig. 5B). The hypothesis that *BicDR* contributes more to the short-distance transport to the base of the shaft and *BicD* more to the long-distance transport to the tip would also explain why *BicDR* bristles tend to be thinner in the proximal region close to the bristle base and *BicD* bristles thicker than the wild type. In the former situation, bristle construction factors would not make it into the bristle shaft, in the latter, they would be moved to the base of the bristle but fail to be transported away from the base.

spn-F is needed for the localization of Hook at the bristle tip (Bitan et al., 2010b) and *hook* is not only required for endocytic trafficking within the eye and the nervous system but also at the bristle tip. Since there is evidence that endocytosis is responsible for the polarized transfer of lipids and membrane proteins, which again is necessary for the polarization of the bristle cell (Rodriguez-Boulán et al., 2005), our results point to an important contribution of *BicD* and *BicDR* to bristle development by localizing Spn-F to the tip. With Spn-F also being part of the IKKε-jvl complex, which regulates the shuttling movement of recycling endosomes and cytoskeletal organization (Otani et al., 2015), the lack of Spn-F in this complex would interfere with the

shuttling regulation of motor proteins at the molecular signaling centers (Otani et al., 2015). This also prevents the transport of Rab-positive vesicles. Mutations in *Rab6* and *Rab11*, members of the Rab protein family that mediate intracellular vesicle trafficking, lead to impaired bristle growth (Purcell and Artavanis-Tsakonas, 1999); (Khodosh et al., 2006; Zhang et al., 2007) and a *rab6* bristle phenotype has been described that matches the bristle phenotype of *BicD^{PA66}/-*; *BicDR⁷¹/+* flies even at the SEM level (Fig. 2H and (Purcell and Artavanis-Tsakonas, 1999). The accumulation of Rab6 signal at the bristle tip is in line with the description of the distal tip being the signaling center for bristle elongation and thereby the most dynamic part of the polarized cell (Otani et al., 2015). Reduced Rab6 levels at the distal tip in hemizygous *BicD* hypomorphs with either one or two functional copies of *BicDR* indicates that the exo- and endocytosis at the bristle tip is impaired. Because Rab6 levels are strongly reduced in these mutants (Figs 4C, S5), it is not clear whether the reduced Rab6 levels, reduced tip localization, or both lead to the observed phenotype. However, because bristle growth takes place in different parts of the bristle⁷⁶, it seems that both defects could interfere with normal bristle formation.

Rab11 contributes to the construction of the bristle by inserting chitin synthase into the plasma membrane thereby allowing bristle chitinization (Adler, 2020). With a complete lack of chitin synthase in *Rab11*⁻ bristles, the bristles not only appear shorter but collapse completely. Even *BicD*; *BicDR* double mutants did not show significant length differences in bristle length during the pupal stage, suggesting that the limiting step in these animals is the construction of the final macrochaetae with their complete chitinization. Because the Rab11 phenotype is quite different from the *BicD*; *BicDR* double mutant bristle phenotype, we did not focus on possible interactions with Rab11. However, the knowledge gained from this study might also be able to explain the *BicD*; *BicDR* double mutant bristle phenotype by a requirement for proper Rab11 localization in the bristle shaft and tip. Reduced transport of Rab11 (or a co-factor) toward the tip might cause a polar reduction of chitin incorporation towards the tip, causing an increased probability of breakage in the distal parts under reduced *BicD* and *BicDR* activity.

Actin modules in the bristle shaft are central to the construction of the bristle. The disorganized F-actin network seen in the mutants (Fig. 4B) can either be caused by insufficient build-up, maintenance, or stability of the F-actin, resulting in fragmented actin bundles or incorrect alignment of already formed bundles. These defects can be expected to prevent normal chitinization. Future research should address whether defects in Arp2/3 or Rab vesicle transport and localization cause the defective actin bundles and whether this affects chitinization and bristle shaft stability and causes shorter and thinner bristles.

Our results demonstrate how directed transport contributes to the organization of elongated and asymmetric cells. The microtubule transport, which localizes factors that organize cellular functions, connects directly and indirectly to vesicle trafficking and the stability of the actin cytoskeleton. We showed that *BicD* and *BicDR* contribute together to this directed transport and the development of the long bristles in a partially redundant manner. Our results led to the hypothesis that *BicD* might be more specialized for long-haul transport and *BicDR* more for short-distance, local transport. Future studies should test this hypothesis.

Materials and Methods

Fly stocks and genetics

Flies were kept and bred on standard cornmeal agar containing yeast, sucrose, potassium sodium tartrate, methylparaben, and propionic acid. For the crosses, multiple virgins (5 to 10) were added to several males (3 to 5) and incubated at 25°C. Fly strains used are listed in Table S3. *BicD*^{PA66} (*BicD*^{A40V} (Schüpbach and Wieschaus, 1991; Suter and Steward, 1991)), *BicDR*^(rev), *BicDR*²⁹, *BicDR*⁵¹, and *BicDR*⁷¹. Standard methods were used to generate *BicDR* excision stocks with the two *P* elements *P{SUPor-P}* and *P{RS5}* (Bellen et al., 2004; Ryder et al., 2004). The excisions were characterized molecularly by extracting DNA from heterozygous mutant males followed by PCR with primers framing the deleted regions of the *BicDR* gene. The screening by PCR revealed that two excision stocks are missing a fragment around the insertion site of the *P*-elements *P{SUPor-P}*: *BicDR*²⁹, *BicDR*⁵¹, and one around the insertion site of *P{RS5}*: *BicDR*⁷¹. These stocks were double-balanced and kept for further examinations. In the case of the mutant *BicDR*^(rev), the activated *P*-element *P{RS5}* reverted the genomic sequence of the *BicDR* gene to the wild-type sequence when it jumped out. The wild-type revertant *BicDR*^(rev) was used as a control for the excision mutants.

v; *CyO/Sp* flies were kindly provided by Simon Bullock. Stocks from the Vienna Drosophila RNAi Center (VDRC) and the Bloomington Stock Center are listed in the appendix. For tissue-specific knock-down or gene expression, the *UAS-Gal4* system was used (Brand and Perrimon, 1993).

CRISPR/Cas9 and generation of transgenic flies

All gRNAs were designed manually and verified on the web-based tool called *CRISPR optimal target finder*. The gRNAs for attaching a GFP-tag (5'-ATTATCGCTGAAATAAACTC-3') and the gRNA for the deletion and substitution of K555 (5'-AGTCCATTCAGCAAAAGG-3') were cloned

into pCFD5 plasmids following the “gRNA cloning protocol for cloning single gRNA plasmids” (Port and Bullock, 2016). Transgenic flies were generated using the ΦC31- based integration system (Bischof et al., 2007) and crossed with *nos-Cas9* expressing animals.

To add a GFP-tag to the C-terminus of the BicDR protein, the appropriate *eGFP* DNA sequence (Tsien, 1998) with a linker and two 1,200 bp long arms homologous to the *BicDR* gene and framing the stop codon were cloned into a pBluescript II SK (+) vector. The construct was injected into embryos with the genotype *w, y, w⁺ nos-Cas9/Y; gRNA v⁺/+; BicDR*/BicDR**. To generate the *BicDR^{K555A}::GFP* mutant, the sequence within the template vector was modified by site-directed mutagenesis before injection. All constructs were sequence verified. All primers used for DNA construction are listed in Table S4.

Genetic interaction assay

In the following crossing schemes *BicDR** indicates one of the excisions, *BicDR²⁹*, *BicDR⁵¹*, and *BicDR⁷¹*, the deletion mutant *BicDR^{8.1}*, the *BicDR^{null}* allele *Df737 (BicDR^{Df})* or the wild-type revertant *BicDR^(rev)*.

♀ *w; BicD^{PA66}/CyO; BicDR* / TM6B* x *w; Df7068/CyO; Df4515/TM3, Sb* ♂

For every cross, 30 virgins with the above genotype were added to 15 males. Every two days, the flies were transferred to a new plastic bottle. The frequency of every genotype of the progeny was determined. The progeny was also sorted by sex and genotype and kept at 18°C for the following experiments. Females who were not virgins anymore were dissected, and their ovaries were stained. The frequency of genotypes of eclosed flies from each cross was counted for 9 days each. All statistics and graphics were done using the GraphPad Prism 5 software.

Analysis of bristle development

The following crosses were used to determine the severity of the *BicDR* alleles and their interaction with *BicD*:

♀ *w; BicD^{PA66}/CyO; BicDR* / TM6B* x *Df7068/SM6B* ♂ → *w; BicD^{PA66}/Df7068; BicDR* /+*

♀ *w; BicD^{PA66}/CyO ftz lacZ* x *w; Df7068/CyO; Df4515, w⁺/TM3, Sb* ♂ → *w; BicD^{PA66}/Df7068; Df4515, w⁺/+*

To investigate the bristle phenotype further, pupae with the following genotypes were dissected and stained following the protocol by Tilney et al. (Tilney et al., 1998) The outline of the bristle

cell was estimated from the distribution of the actin bundles and the cell body from the position of the root (basis) of the actin bundles (i.e., the cell body of the bristle cell is expected to be directly beneath the first actin bundles).

♀ w; *BicD*^{PA66}/CyO, Act-GFP; *BicDR**/TM6B, Tb x Df7068/CyO, Act-GFP ♂

→ w; *BicD*^{PA66}/Df7068; *BicDR**/+

→ w; *BicD*^{PA66}/Df7068; TM6B, Tb/+

Immunostaining and microscopy

Dechorionated embryos or dissected tissue that was kept on ice for less than 30 minutes were fixed in 4% paraformaldehyde for 20 minutes and blocked with either 5% milk or bovine serum albumin (Fraction V) for 2 hours at room temperature. Primary antibodies were incubated overnight, followed by washing steps and incubation with secondary antibodies for at least 2 hours. Primary antibodies were diluted as follows: anti-GFP (rabbit, 1:200, ImmunoKontakt), anti-GFP (mouse, 1:200), anti-Ef1 γ (rat, 1:1,000; (Serpinskaya et al., 2014), anti-Rab6 (rabbit and guinea pig, 1:200) (Iwanami et al., 2016), anti-Spn-F (rabbit, 1:300, DSHB), anti-Asense (guinea pig, 1:100; (Brand et al., 1993). Secondary antibodies were Alexa Fluor 488 (anti-rabbit 1:800), Alexa Fluor 488 Plus (anti-rabbit, 1:200), Alexa Fluor 647 (anti-mouse, 1:200), Alexa Fluor 647 Plus (anti-rabbit, 1:200), Cy3 (anti-mouse, 1:400). The images were taken with a Leica TCS-SP8 confocal laser-scanning microscope and processed using the FIJI software.

Scanning electron microscopy of bristles

Flies were anesthetized with CO₂, decapitated, mounted, and coated with gold. Scanning was performed on a Zeiss Gemini 450 SEM with electron high tension set to 5 kV. Signals were detected with detectors for secondary electrons (and backscattered electrons). For measuring the length of the bristles, only apparently intact bristles that were mounted relatively horizontally were considered. In all cases, only the length of the longer pSC bristles was recorded because these were apparently the ones that were mounted more horizontally and the measurements on the pictures can be expected to be more accurate.

Isolation of embryonic BicDR complexes for mass spectrometry

12-16 hours old embryos were collected and lysed in homogenization buffer (25 mM Hepes pH 7.4; 150mM NaCl; 0.5mM EDTA pH 8.0; 1 mM DTT and 1 tablet of proteinase inhibitor cocktail; Roche 11836170001). The aqueous phase of the lysate was collected after 1 hour of centrifugation at 4°C and centrifuged again for 25 minutes. Subsequently, one part of the aqueous phase was saved as input control, while the rest was incubated with Plus Sepharose G beads that were coated with anti-GFP antibody overnight at 4°C. 5-7 washing steps with wash buffer (25 mM Hepes pH 7.4; 150mM NaCl; 0.5mM EDTA pH 8.0; 1 mM DTT and ½ tablet of proteinase inhibitor cocktail, Roche 11836170001) were performed before the beads were either sent for mass spectrometry or prepared with the appropriate amount of SDS for SDS-PAGE and Western blot analysis. SDS/PAGE bands that were present in the IP from the BicDR::GFP fusion protein were cut out of the gel and sent directly for mass spectrometry. As a control, the equivalent regions of the control lanes were also cut out and used for a mass spectrometric analysis.

Yeast two-hybrid assay

The full-length cDNA of *BicDR* and *Ef1γ* as well as the C-terminal domain (CTD) of *BicDR* were cloned into pOAD and pOBD2 vectors so that they were in frame with the activator domain (AD) or the DNA binding domain (BD) (Cagney et al., 2000; Vazquez-Pianzola et al., 2022). In this way, BicDR-AD, BicDR-CTD-AD, Ef1γ-AD, as well as BicDR-BD, BicDR-CTD-BD, and Ef1γ-BD were created. The BicD-AD and Egl-AD, as well as BicD-BD and Egl-BD, have been described previously (Vazquez-Pianzola et al., 2022).

Acknowledgments

We thank S. Bullock, L. Rabinow, A. K. Satoh, U. Abdu, the Bloomington *Drosophila* Stock Center (NIH P400D018537), and the Developmental Studies Hybridoma Bank (created by the NICHD of the NIH and maintained at The University of Iowa, Department of Biology, Iowa City, IA 52242) for constructs, fly stocks and antibodies. We thank FlyBase (U41HG000739) for the *Drosophila* genomic resources. We wish to thank B. Frey from the DCBP (University of Bern) for her extremely helpful and competent electron microscopy work and C. Elci for fly food and stock maintenance.

Funding

This work was supported by funds from the Swiss National Science Foundation (SNF, project grants 31003A_173188 and 310030_205075; www.snf.ch) and the University of Bern (www.unibe.ch) to BS.

Data availability

All relevant data can be found within the article and its supplementary information.

References

- Abdelilah-Seyfried, S., Chan, Y.M., Zeng, C., Justice, N.J., Younger-Shepherd, S., Sharp, L.E., Barbel, S., Meadows, S.A., Jan, L.Y., Jan, Y.N., 2000. A gain-of-function screen for genes that affect the development of the drosophila adult external sensory organ. *Genetics* 155, 733–752. <https://doi.org/10.1093/genetics/155.2.733>
- Abdu, U., Bar, D., Schüpbach, T., 2006. spn-F encodes a novel protein that affects oocyte patterning and bristle morphology in *Drosophila*. *Development* 133, 1477–1484. <https://doi.org/10.1242/dev.02319>
- Adler, P.N., 2020. The localization of chitin synthase mediates the patterned deposition of chitin in developing *Drosophila* bristles. *bioRxiv* 718841. <https://doi.org/10.1101/718841>
- Aradska, J., Bulat, T., Sialana, F.J., Birner-Gruenberger, R., Erich, B., Lubec, G., 2015. Gel-free mass spectrometry analysis of *Drosophila melanogaster* heads. *Proteomics* 15, 3356–3360. <https://doi.org/10.1002/pmic.201500092>
- Bagley, J.A., Yan, Z., Zhang, W., Wildonger, J., Jan, L.Y., Jan, Y.N., 2014. Double-Bromo and Extraterminal (BET) domain proteins regulate dendrite morphology and mechanosensory function. *Genes Dev* 28, 1940–1956. <https://doi.org/10.1101/gad.239962.114>
- Bartolini, F., Gundersen, G.G., 2006. Generation of noncentrosomal microtubule arrays. *J Cell Sci* 119, 4155–4163. <https://doi.org/10.1242/jcs.03227>
- Bellen, H.J., Levis, R.W., Liao, G., He, Y., Carlson, J.W., Tsang, G., Evans-Holm, M., Hiesinger, P.R., Schulze, K.L., Rubin, G.M., Hoskins, R.A., Spradling, A.C., 2004. The BDGP Gene Disruption Project. *Genetics* 167, 761–781. <https://doi.org/10.1534/genetics.104.026427>

- Berdnik, D., Török, T., González-Gaitán, M., Knoblich, J.A., 2002. The endocytic protein α -adaptin is required for numb-mediated asymmetric cell division in *Drosophila*. *Dev Cell* 3, 221–231. [https://doi.org/10.1016/S1534-5807\(02\)00215-0](https://doi.org/10.1016/S1534-5807(02)00215-0)
- Bischof, J., Maeda, R.K., Hediger, M., Karch, F., Basler, K., 2007. An optimized transgenesis system for *Drosophila* using germ-line-specific ϕ C31 integrases. *Proc Natl Acad Sci U S A* 104, 3312–3317. <https://doi.org/10.1073/pnas.0611511104>
- Bitan, A., Guild, G.M., Abdu, U., 2010a. The highly elongated drosophila mechanosensory bristle. *Fly (Austin)* 4, 246–248. <https://doi.org/10.4161/fly.4.3.12174>
- Bitan, A., Guild, G.M., Bar-Dubin, D., Abdu, U., 2010b. Asymmetric microtubule function is an essential requirement for polarized organization of the *Drosophila* bristle. *Mol Cell Biol* 30, 496–507. <https://doi.org/10.1128/MCB.00861-09>
- Brand, A.H., Perrimon, N., 1993. Targeted gene expression as a means of altering cell fates and generating dominant phenotypes. *Development* 118, 401–415. <https://doi.org/10.1242/dev.118.2.401>
- Brand, M., Jarman, A.P., Jan, L.Y., Jan, Y.N., 1993. asense is a *Drosophila* neural precursor gene and is capable of initiating sense organ formation. *Development* 119, 1–17. <https://doi.org/10.1242/dev.119.1.1>
- Cagney, G., Uetz, P., Fields, S., 2000. High-throughput screening for protein-protein interactions using two-hybrid assay. *Methods Enzymol* 328, 3–14. [https://doi.org/10.1016/s0076-6879\(00\)28386-9](https://doi.org/10.1016/s0076-6879(00)28386-9)
- Casad, M.E., Abraham, D., Kim, I.M., Frangakis, S., Dong, B., Lin, N., Wolf, M.J., Rockman, H.A., 2011. Cardiomyopathy is associated with ribosomal protein gene haplo-insufficiency in *Drosophila melanogaster*. *Genetics* 189, 861–870. <https://doi.org/10.1534/genetics.111.131482>
- Chaaban, S., Carter, A.P., 2022. Structure of dynein–dynactin on microtubules shows tandem adaptor binding. *Nature* 1–5. <https://doi.org/10.1038/s41586-022-05186-y>
- Chihara, T., Kato, K., Taniguchi, M., Ng, J., Hayashi, S., 2003. Rac promotes epithelial cell rearrangement during tracheal tubulogenesis in *Drosophila*. *Development*. <https://doi.org/10.1242/dev.00361>
- Claußen, M., Suter, B., 2005. BicD-dependent localization processes: from *Drosophila* development to human cell biology. *Annals of Anatomy - Anatomischer Anzeiger* 187, 539–553. <https://doi.org/10.1016/J.AANAT.2005.07.004>
- CRISPR Optimal Target Finder [WWW Document], n.d. URL <http://tools.flycrispr.molbio.wisc.edu/targetFinder/> (accessed 1.18.19).

- Dienstbier, M., Boehl, F., Li, X., Bullock, S.L., 2009. Egalitarian is a selective RNA-binding protein linking mRNA localization signals to the dynein motor. *Genes Dev* 23, 1546–1558. <https://doi.org/10.1101/gad.531009>
- Hart, K., Klein, T., Wilcox, M., 1993. A Minute encoding a ribosomal protein enhances wing morphogenesis mutants. *Mech Dev* 43, 101–110. [https://doi.org/10.1016/0925-4773\(93\)90028-V](https://doi.org/10.1016/0925-4773(93)90028-V)
- Hartenstein, V., 1993. *Atlas of Drosophila Development* by Volker Hartenstein.
- Iwanami, N., Nakamura, Y., Satoh, T., Liu, Z., Satoh, A.K., 2016. Rab6 Is Required for Multiple Apical Transport Pathways but Not the Basolateral Transport Pathway in Drosophila Photoreceptors. *PLoS Genet* 12, e1005828. <https://doi.org/10.1371/journal.pgen.1005828>
- Januschke, J., Nicolas, E., Compagnon, J., Formstecher, E., Goud, B., Guichet, A., 2007. Rab6 and the secretory pathway affect oocyte polarity in Drosophila. *Development* 134, 3419–3425. <https://doi.org/10.1242/dev.008078>
- Jenkins, V.K., Larkin, A., Thurmond, J., 2022. Using FlyBase: A Database of Drosophila Genes and Genetics, in: *Methods in Molecular Biology*. Humana Press Inc., pp. 1–34. https://doi.org/10.1007/978-1-0716-2541-5_1
- Khodosh, R., Augsburger, A., Schwarz, T.L., Garrity, P.A., 2006. Bchs, a BEACH domain protein, antagonizes Rab11 in synapse morphogenesis and other developmental events. *Development* 133, 4655–4665. <https://doi.org/10.1242/dev.02650>
- Kim, S., Kellner, J., Lee, C.H., Coulombe, P.A., 2007. Interaction between the keratin cytoskeleton and eEF1By affects protein synthesis in epithelial cells. *Nat Struct Mol Biol* 14, 982–983. <https://doi.org/10.1038/nsmb1301>
- Koch, R., Ledermann, R., Urwyler, O., Heller, M., Suter, B., 2009. Systematic Functional Analysis of Bicaudal-D Serine Phosphorylation and Intragenic Suppression of a Female Sterile Allele of BicD. *PLoS One* 4, e4552. <https://doi.org/10.1371/journal.pone.0004552>
- Kong, J., Han, H., Bergalet, J., Bouvrette, L.P.B., Hernández, G., Moon, N.S., Vali, H., Lécuyer, É., Lasko, P., 2019. A ribosomal protein S5 isoform is essential for oogenesis and interacts with distinct RNAs in Drosophila melanogaster. *Sci Rep* 9. <https://doi.org/10.1038/s41598-019-50357-z>
- Leiss, F., Koper, E., Hein, I., Fouquet, W., Lindner, J., Sigrist, S., Tavosanis, G., 2009. Characterization of dendritic spines in the Drosophila central nervous system. *Dev Neurobiol* 69, 221–234. <https://doi.org/10.1002/dneu.20699>

- Le Bras, S., Rondanino, C., Kriegel-Taki, G., raldine, Dussert, A., Borgne, R. Le, 2012. Genetic identification of intracellular trafficking regulators involved in Notch-dependent binary cell fate acquisition following asymmetric cell division. *J Cell Sci* 125, 4886–4901.
<https://doi.org/10.1242/jcs.110171>
- Marygold, S.J., Roote, J., Reuter, G., Lambertsson, A., Ashburner, M., Millburn, G.H., Harrison, P.M., Yu, Z., Kenmochi, N., Kaufman, T.C., Leever, S.J., Cook, K.R., 2007. The ribosomal protein genes and Minute loci of *Drosophila melanogaster*. *Genome Biol* 8, 1–26.
<https://doi.org/10.1186/gb-2007-8-10-r216>
- Melkov, A., Baskar, R., Alcalay, Y., Abdu, U., 2016. A new mode of mitochondrial transport and polarized sorting regulated by Dynein, Milton and Miro. *Development (Cambridge)* 143, 4203–4213. <https://doi.org/10.1242/dev.138289>
- Nagaraj, R., Adler, P.N., 2012. Dusky-like functions as a Rab11 effector for the deposition of cuticle during *Drosophila* bristle development. *Development* 139, 906–916.
<https://doi.org/10.1242/dev.074252>
- Otani, T., Oshima, K., Kimpara, A., Takeda, M., Abdu, U., Hayashi, S., 2015. A transport and retention mechanism for the sustained distal localization of Spn-F–IKK ϵ during *Drosophila* bristle elongation. *Development (Cambridge)* 142, 2338–2351.
<https://doi.org/10.1242/dev.121863>
- Peña-Rangel, M.T., Rodriguez, I., Riesgo-Escovar, J.R., 2002. A Misexpression Study Examining Dorsal Thorax Formation in *Drosophila melanogaster*. *Genetics* 160, 1035–1050.
<https://doi.org/10.1093/genetics/160.3.1035>
- Pirraglia, C., Jattani, R., Myat, M.M., 2006. Rac function in epithelial tube morphogenesis. *Dev Biol* 290, 435–446. <https://doi.org/10.1016/j.ydbio.2005.12.005>
- Port, F., Bullock, S.L., 2016. Augmenting CRISPR applications in *Drosophila* with tRNA-flanked sgRNAs. *Nat Methods* 13, 852–854. <https://doi.org/10.1038/nmeth.3972>
- Purcell, K., Artavanis-Tsakonas, S., 1999. The developmental role of warthog, the notch modifier encoding Drab6. *J Cell Biol* 146, 731–40. <https://doi.org/10.1083/jcb.146.4.731>
- Ran, B., Bopp, R., Suter, B., 1994. Null alleles reveal novel requirements for Bic-D during *Drosophila* oogenesis and zygotic development. *Development* 120, 1233–1242.
<https://doi.org/10.1242/dev.120.5.1233>
- Rodriguez-Boulan, E., Kreitzer, G., Müsch, A., 2005. Organization of vesicular trafficking in epithelia. *Nat Rev Mol Cell Biol*. <https://doi.org/10.1038/nrm1593>

- Ryder, E., Blows, F., Ashburner, M., Bautista-Llacer, R., Coulson, D., Drummond, J., Webster, J., Gubb, D., Gunton, N., Johnson, G., O'Kane, C.J., Huen, D., Sharma, P., Asztalos, Z., Baisch, H., Schulze, J., Kube, M., Kittlaus, K., Reuter, G., Maroy, P., Szidonya, J., Rasmuson-Lestander, A., Ekström, K., Dickson, B., Hugentobler, C., Stocker, H., Hafen, E., Lepesant, J.A., Pflugfelder, G., Heisenberg, M., Mechler, B., Serras, F., Corominas, M., Schneuwly, S., Preat, T., Roote, J., Russell, S., 2004. The DrosDel Collection. *Genetics* 167, 797–813.
<https://doi.org/10.1534/genetics.104.026658>
- Sanghavi, P., Liu, G., Veeranan-Karmegam, R., Navarro, C., Gonsalvez, G.B., 2016. Multiple roles for egalitarian in polarization of the *Drosophila* egg chamber. *Genetics* 203, 415–432.
<https://doi.org/10.1534/genetics.115.184622>
- Schlager, M.A., Kapitein, L.C., Grigoriev, I., Burzynski, G.M., Wulf, P.S., Keijzer, N., de Graaff, E., Fukuda, M., Shepherd, I.T., Akhmanova, A., Hoogenraad, C.C., 2010. Pericentrosomal targeting of Rab6 secretory vesicles by Bicaudal-D-related protein 1 (BICDR-1) regulates neuritogenesis. *EMBO J* 29, 1637–51. <https://doi.org/10.1038/emboj.2010.51>
- Schüpbach, T., Wieschaus, E., 1991. Female sterile mutations on the second chromosome of *Drosophila melanogaster*. II. Mutations blocking oogenesis or altering egg morphology. *Genetics* 129, 1119–36.
- Serpinskaya, A.S., Tophile, K., Rabinow, L., Gelfand, V.I., 2014. Protein kinase Darkener of apricot and its substrate EF1 γ regulate organelle transport along microtubules. *J Cell Sci* 127, 33–39.
<https://doi.org/10.1242/jcs.123885>
- Splinter, D., Razafsky, D.S., Schlager, M.A., Serra-Marques, A., Grigoriev, I., Demmers, J., Keijzer, N., Jiang, K., Poser, I., Hyman, A.A., Hoogenraad, C.C., King, S.J., Akhmanova, A., 2012. BICD2, dynactin, and LIS1 cooperate in regulating dynein recruitment to cellular structures. *Mol Biol Cell* 23, 4226–4241. <https://doi.org/10.1091/mbc.E12-03-0210>
- Suter, B., 2018. RNA localization and transport. *Biochimica et Biophysica Acta (BBA) - Gene Regulatory Mechanisms*. <https://doi.org/10.1016/J.BBAGRM.2018.08.004>
- Suter, B., Steward, R., 1991. Requirement for phosphorylation and localization of the Bicaudal-D protein in *Drosophila* oocyte differentiation. *Cell* 67, 917–26. [https://doi.org/10.1016/0092-8674\(91\)90365-6](https://doi.org/10.1016/0092-8674(91)90365-6)
- Takano, T.S., 1998. Loss of Notum Macrochaetae as an Interspecific Hybrid Anomaly Between *Drosophila melanogaster* and *D. simulans*. *Genetics* 149, 1435–1450.
<https://doi.org/10.1093/genetics/149.3.1435>

- Thurmond, J., Goodman, J.L., Strelets, V.B., Attrill, H., Gramates, L.S., Marygold, S.J., Matthews, B.B., Millburn, G., Antonazzo, G., Trovisco, V., Kaufman, T.C., Calvi, B.R., Perrimon, N., Gelbart, S.R., Agapite, J., Broll, K., Crosby, L., Santos, G. dos, Emmert, D., Gramates, L.S., Falls, K., Jenkins, V., Matthews, B., Sutherland, C., Tabone, C., Zhou, P., Zytkevich, M., Brown, N., Antonazzo, G., Attrill, H., Garapati, P., Holmes, A., Larkin, A., Marygold, S., Millburn, G., Pilgrim, C., Trovisco, V., Urbano, P., Kaufman, T., Calvi, B., Czoch, B., Goodman, J., Strelets, V., Thurmond, J., Cripps, R., Baker, P., 2019. FlyBase 2.0: the next generation. *Nucleic Acids Res* 47, D759–D765. <https://doi.org/10.1093/nar/gky1003>
- Tilney, L.G., Connelly, P., Smith, S., Guild, G.M., 1996. F-actin bundles in *Drosophila* bristles are assembled from modules composed of short filaments. *Journal of Cell Biology* 135, 1291–1308. <https://doi.org/10.1083/jcb.135.5.1291>
- Tilney, L.G., Connelly, P.S., Vranich, K.A., Shaw, M.K., Guild, G.M., 1998. Why are two different cross-linkers necessary for actin bundle formation in vivo and what does each cross-link contribute? *J Cell Biol* 143, 121–33. <https://doi.org/10.1083/JCB.143.1.121>
- Tsien, R.Y., 1998. The green fluorescent protein. *Annu Rev Biochem*. <https://doi.org/10.1146/annurev.biochem.67.1.509>
- Urnavicius, L., Lau, C.K., Elshenawy, M.M., Morales-Rios, E., Motz, C., Yildiz, A., Carter, A.P., 2018. Cryo-EM shows how dynactin recruits two dyneins for faster movement. *Nature* 554, 202–206. <https://doi.org/10.1038/nature25462>
- Vanolst, L., Fromental-Ramain, C., Ramain, P., 2005. Toutatis, a TIP5-related protein, positively regulates Pannier function during *Drosophila* neural development. *Development* 132, 4327–4338. <https://doi.org/10.1242/dev.02014>
- Vazquez-Pianzola, P., Adam, J., Haldemann, D., Hain, D., Urlaub, H., Suter, B., 2014. Clathrin heavy chain plays multiple roles in polarizing the *Drosophila* oocyte downstream of Bic-D. *Development* 141, 1915–26. <https://doi.org/10.1242/dev.099432>
- Vazquez-Pianzola, P., Beuchle, D., Saro, G., Hernández, G., Maldonado, G., Brunßen, D., Meister, P., Suter, B., 2022. Female meiosis II and pronuclear fusion require the microtubule transport factor Bicaudal D. *Development* 149. <https://doi.org/10.1242/dev.199944>
- Vazquez-Pianzola, P., Urlaub, H., Suter, B., 2011. Pabp binds to the *osk* 3'UTR and specifically contributes to *osk* mRNA stability and oocyte accumulation. *Dev Biol* 357, 404–418. <https://doi.org/10.1016/j.ydbio.2011.07.009>

- Zhang, J., Fonovic, M., Suyama, K., Bogyo, M., Scott, M.P., 2009. Rab35 controls actin bundling by recruiting fascin as an effector protein. *Science* (1979) 325, 1250–1254.
<https://doi.org/10.1126/science.1174921>
- Zhang, J., Schulze, K.L., Hiesinger, P.R., Suyama, K., Wang, S., Fish, M., Acar, M., Hoskins, R.A., Bellen, H.J., Scott, M.P., 2007. Thirty-One Flavors of *Drosophila* Rab Proteins. *Genetics* 176, 1307–1322. <https://doi.org/10.1534/genetics.106.066761>

Figures

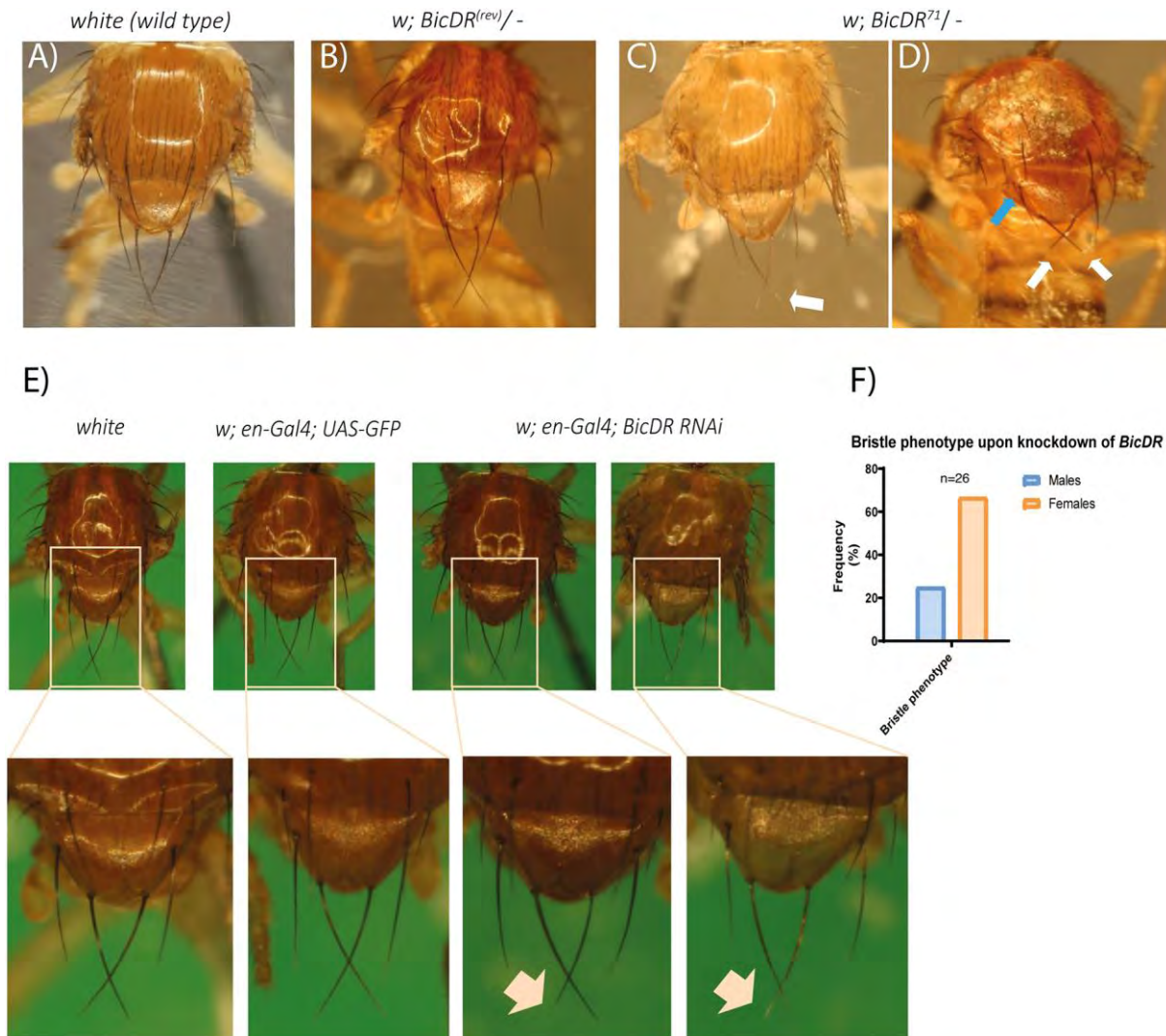


Fig. 1. Bristle phenotypes in *BicDR* mutants (A) Macrochaetae of a wild-type control fly, the revertant *w; BicDR^(rev)/Df4515* (B) and *w; BicDR⁷¹/Df4515* (C and D). Note that the notum of the *w; BicDR^(rev)/Df4515* control does not show any differences compared to the wild type, whereas *w; BicDR⁷¹/Df4515* flies eclosed with shorter pSC macrochaetae (white arrows in D) and occasionally with an additional aSC bristle (blue arrow in D); identification of macrochaetae was according to Takano (1998). (E) RNAi knockdown of *BicDR* induces defective bristles. *w; UAS-BicDR-RNAi/en-Gal4; UAS-BicDR-RNAi/UAS-GFP*. Note the slightly paler macrochaetae tips and occasional shorter macrochaetae marked with an arrow. (F) Mostly female flies eclosed with this knock-down phenotype of *BicDR* (12 out of 18 female and 2 out of 8 male flies).

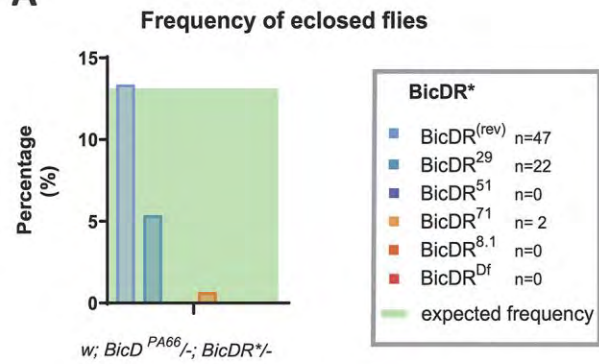
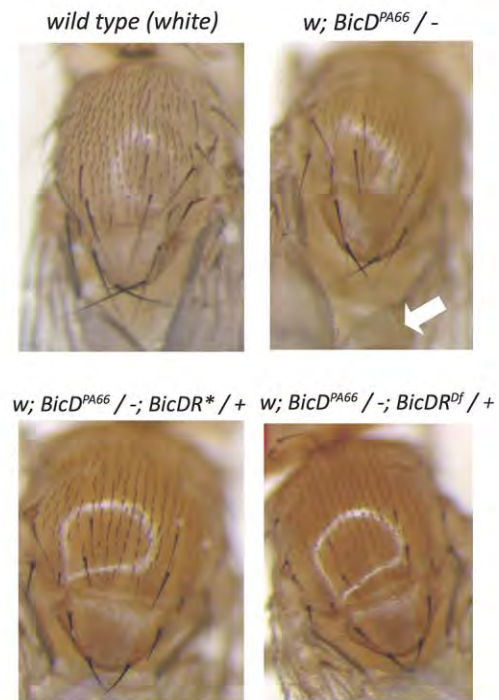
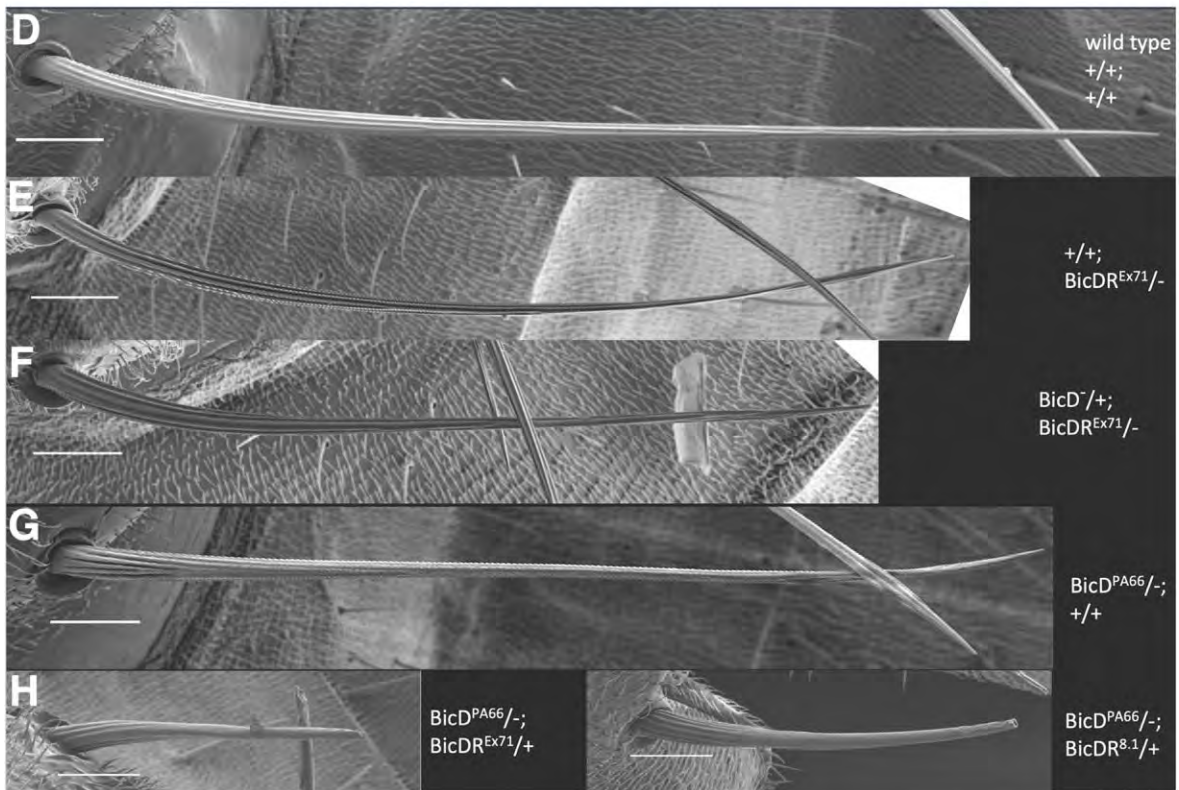
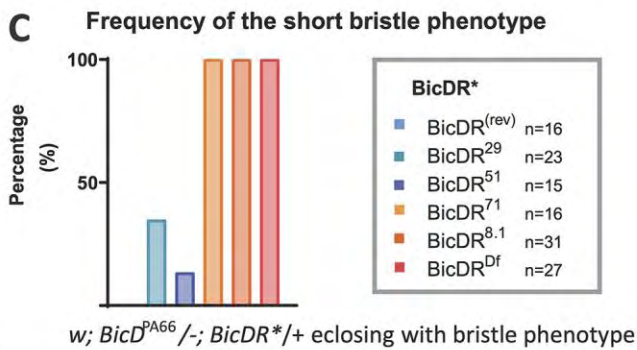
A**B****C**

Fig. 2. (A) Frequency of eclosed *BicD*; *BicDR* double mutants with the genotype *w*; *BicD*^{PA66}/–; *BicDR**/–. Adult flies eclosed only in crosses containing *BicDR*²⁹ or the control *BicDR*^(rev) except for one escaper with the allele *BicDR*⁷¹. All of them developed a short-bristle phenotype. The genotype *w*; *BicD*^{PA66}/–; *Df4515*/+ eclosed in all crosses and all flies with the named genotype developed the short-bristle phenotype as well. The calculated expected frequency is always shown in green. **(B)** Comparison of the bristle phenotypes observed in controls (*white*), *BicD*^{PA66}/–, and *BicD*^{PA66}/–; *BicDR*⁷¹/+, as well as *BicD*^{PA66}/–; *BicDR*^{Df}/+. Note that the *BicD* bristle phenotype, which manifests itself in discolored and brittle bristle tips, deteriorates with the reduction of *BicDR* function. The phenotypes observed in *BicD*^{PA66}/–; *BicDR*⁷¹/+ and *BicD*^{PA66}/–; *BicDR*^{Df}/+ show the same severity, indicating that the allele *BicDR*⁷¹ behaves like a *BicDR*^{null} mutant for this phenotype. **(C)** shows the frequency of the short bristle phenotype in *BicD*^{PA66}/–; *BicDR**/+ animals. The *BicDR*-excisions that the animals carry and the deficiency *Df737* (this deficiency is also referred to as *BicDR*^{Df}), are indicated. **(D)-(H)** Scanning electron micrographs of the posterior scutellar bristles (pSC) of the wild type, *BicD*, and *BicDR* mutants and mutant combinations showing their effects on bristle length and structure. All scale bars represent 30 μm. **(D)** Wild type is an OreR line outcrossed to a *white* line. **(E)** *BicDR*[–] mutants show slightly shorter, thinner bristles that appear flattened. **(F)** With only one normal copy of *BicD*, *BicDR* bristles are again slightly shorter. **(G)** *BicD*^{PA66}/– bristles are only slightly shorter than wild-type bristles, but the enhancement of the phenotype by inactivating one copy of *BicDR* - shown with two unrelated alleles - is very strong **(H)**. Note that in this genotype, the bundle structure is only visible close to the base and gets lost 50 μm distal to the base. “–” indicates that the *BicD* or *BicDR* gene on the indicated chromosome was deleted by a small deficiency (*Df7068* for *BicD* and *Df4514* for *BicDR*).

S5 for 'Blot transparency'). The samples loaded were from stage 13 to 16 embryos, 3rd instar larvae, adult flies, and salivary glands. All were of the genotype *w; BicDR::GFP/Df4515* or the negative control (*white*). The loading control was GAPDH with a size of 35 kDa (see lower blot). BicDR-B::GFP, with a size of 130 kDa was found mostly in adult flies, 3rd instar larvae, and the dissected salivary glands of the 3rd instar larvae, while BicDR-A::GFP with 110 kDa was mostly expressed in late embryos. **(B)** Stage 13 embryos stained for BicDR::GFP (green). The DNA is stained with Hoechst (blue). BicDR::GFP is expressed apically in the cells of salivary glands and cells along the anterior-posterior embryo axis in a metameric pattern. **(C)** Co-staining of BicDR::GFP embryos with the SOP marker Asense (red) and GFP (green) identifies the GFP⁺ cells in the vicinity of elevated Ase staining.

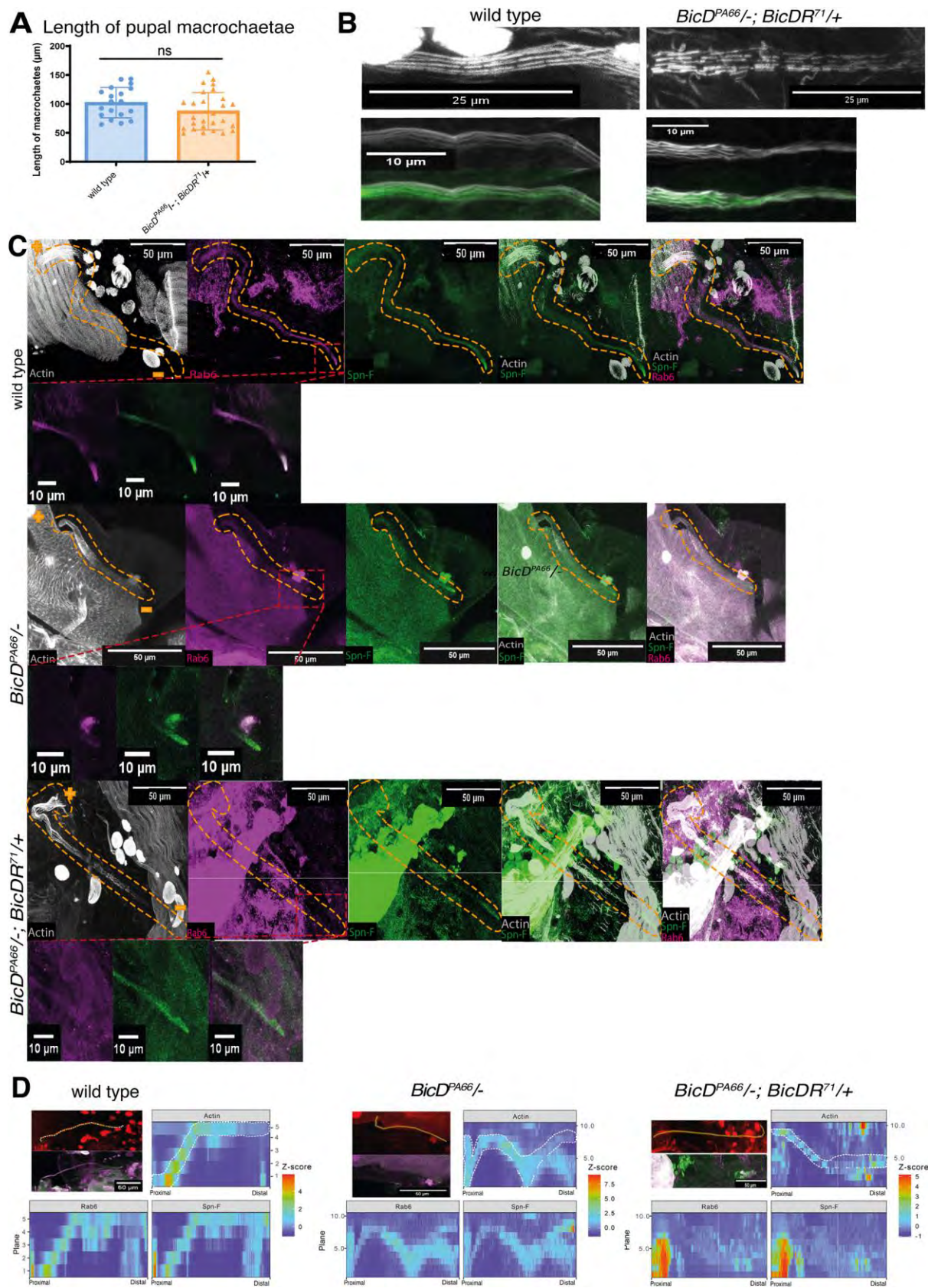


Fig. 4. *BicD*; *BicDR* mutant bristles reach similar lengths in pupae but display irregularly lined up actin bundles in scutellar macrochaetae. (A) The length of single pupal macrochaetae was measured in *white* controls and *BicD*^{PA66}/–; *BicDR*⁷¹/+ double mutants. No significant dissimilarities between the two groups were found at this stage of bristle development. **(B)** Scutellar macrochaetae stained for F-actin and acetylated tubulin in controls and the indicated double mutant (grey: F-actin; green: acetylated tubulin). **(C)** *BicD* and *BicDR* are needed to localize normal levels of Rab6 in the shaft of scutellar macrochaetae and at their bristle tips. This accumulation is impaired in the *BicD*^{PA66}/– and particularly in the *BicD*^{PA66}/–; *BicDR*⁷¹/+ double mutants (grey: F-Actin, green: Spn-F, pink: Rab6; see also Figs 4D, S4, S5 for additional stainings and relative quantification). The genotype of the sample is listed on the left side. All macrochaetae originate in the upper left corner (indicated with a “+”) and grow downwards to the lower right corner (indicated with a “–”). The tip is visualized with the staining for Spn-F. The enlargement of the bristle tips framed by the red boxes in **(C)** is shown for the three channels. The outlines of the bristle cells were estimated from the F-actin staining and the staining for Spn-F and Rab6. The localization of Rab6 decreases toward the bristle tip of *BicD* mutants, while it was completely absent in the distal tips of the *BicD*; *BicDR* double mutants. **(D)** Intensity plots of Rab6 and Spn-F signals in each image plane visualize the distribution of Rab6 and Spn-F signals through the bristle shaft. The highest Z-score of 4 is shown in red, while dark blue marks a Z-score of 0 and indicates that no signal could be detected. The segmented line drawn through the bristle shaft has a width of 10 pixels and their mean result was used for the graphs.

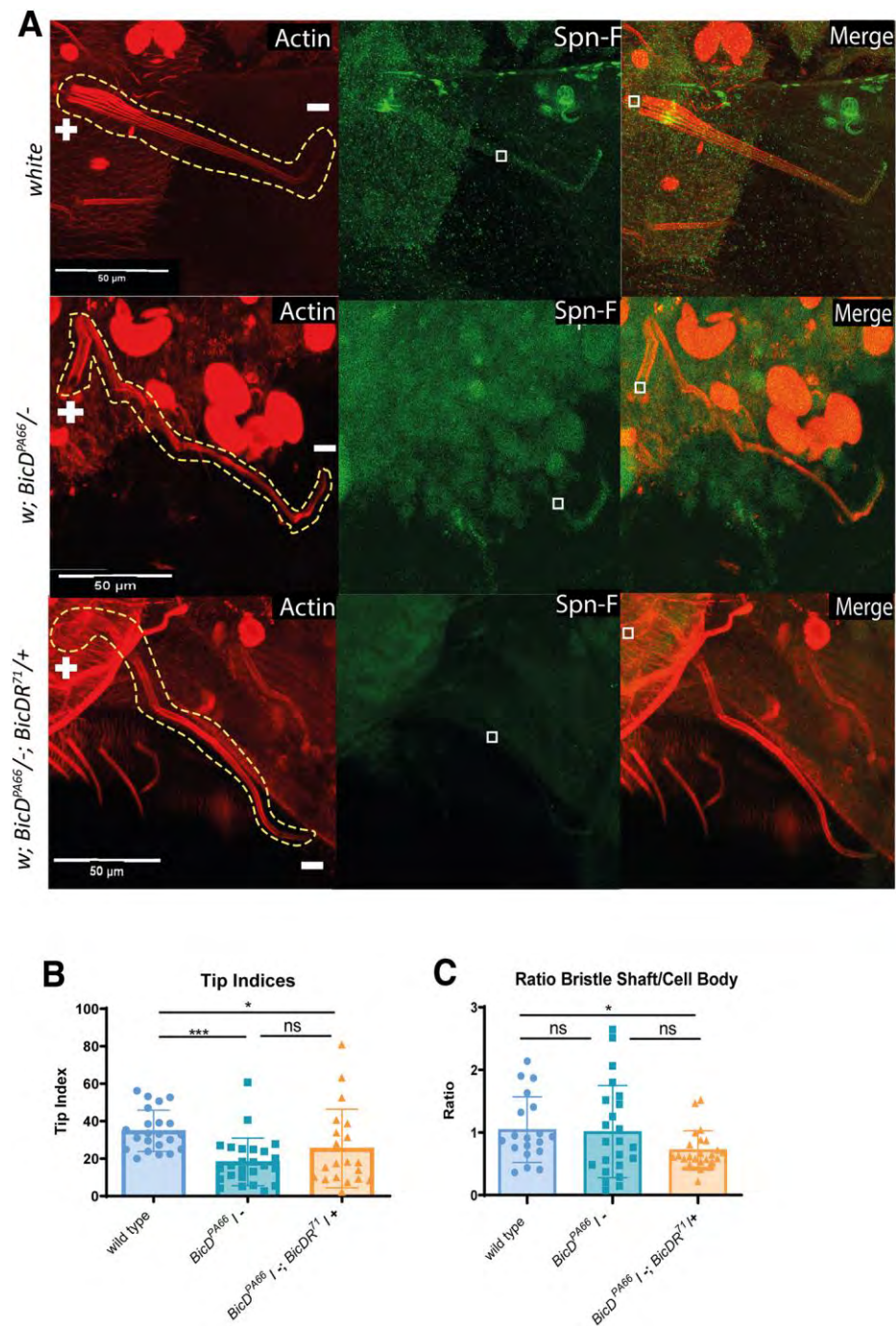


Fig. 5. Pupal bristles of *BicD*; *BicDR* double mutants show impaired Spn-F localization at the bristle tip. (A) Stained macrochaetae (red: F-Actin, green: Spn-F). The genotypes of the samples are listed on the left side. All macrochaetae originate in the upper left corner and have their tips pointing downwards. The localization of Spn-F at the bristle tip is much weaker in *w*;

BicD^{PA66}/Df7068; TM6B/+ and *w*; *BicD^{PA66}/Df7068*; *BicDR⁷¹/+* pupae. This observation could be confirmed with the calculation of the tip index shown in **(B)**. The average tip index of the mutants is significantly lower than those of the control group. **(C)** The ratio of Spn-F signal in the elongated bristle shaft versus its cell body is significantly lower in *BicD^{PA66}/-*; *BicDR^{*}/+* animals. White squares indicate the positions within the bristle shaft where the signal intensity of Spn-F was measured. For the calculation, the signal was measured within one plane in the approximately middle part of the bristle shaft and divided through the signal intensity measured within the plane where the actin bundles sprout out of the tissue.

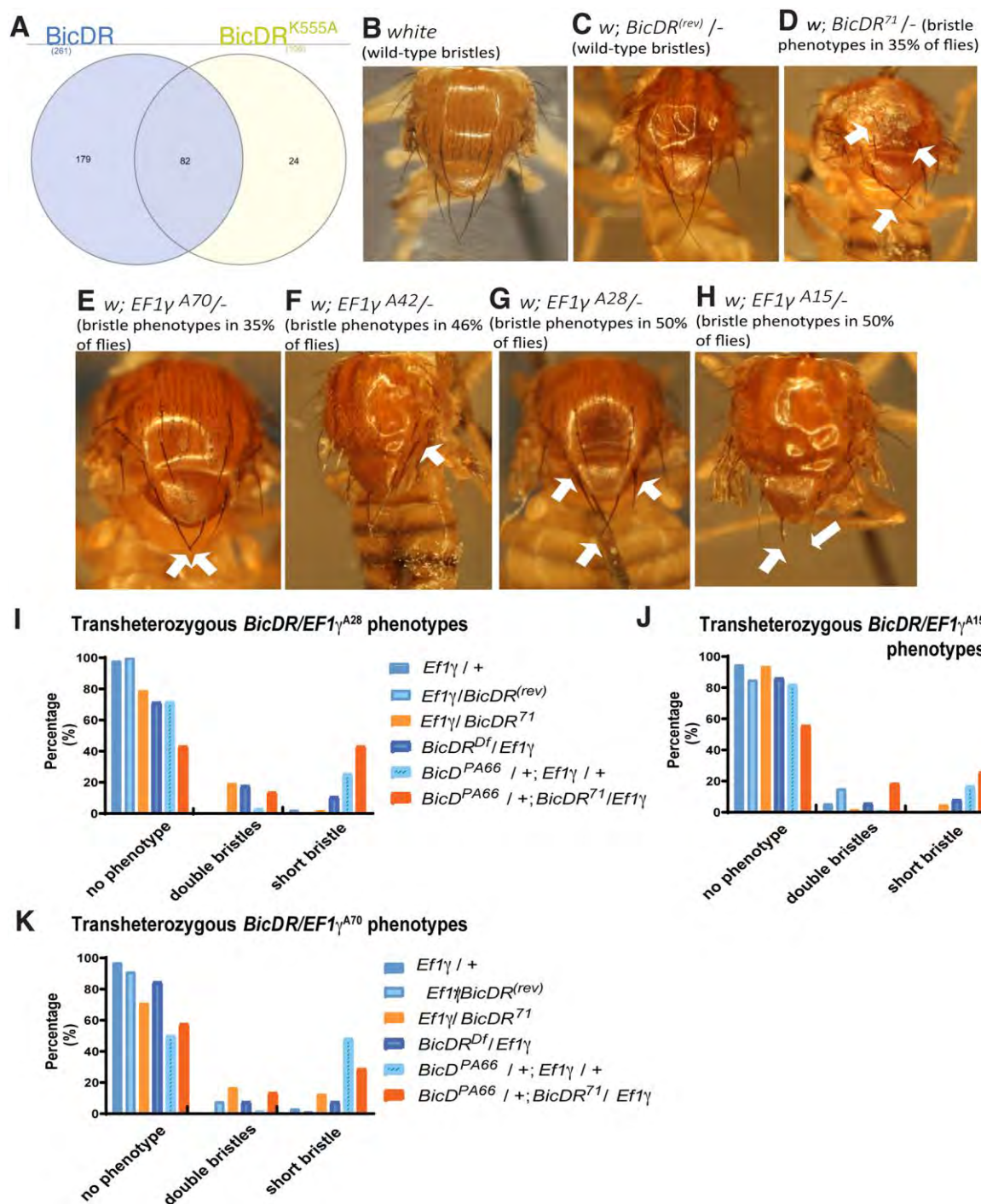


Fig. 6. (A) Proteins identified in the cut-out gel bands from the tagged *BicDR* and *BicDR^{K555A}* immunoprecipitations. (A) A total of 285 potential binding partners were identified. 82 proteins were found in both samples, while 179 proteins were found only in the wild-type *BicDR::GFP* IP. (B)-(H) Resemblance of phenotypes compared to the

(B) *white* control (0% short bristle phenotypes), (C) *BicDR^(rev)/-* control (0% short bristle phenotype), (D) *BicDR⁷¹/-* (35% of flies displayed such a bristle phenotype), (E) *EF1 γ ^{A70}/-* (35% of flies displayed a short bristle phenotype), (F) *EF1 γ ^{A42}/-* (46% of flies eclosed with additional bristles), (G) *EF1 γ ^{A28}/-* (50% of flies had additional and shorter bristles), (H) *EF1 γ ^{A15}/-* (50% of flies had shorter bristles). Note that the *white* control and 93% of the *BicDR revertants*, *BicDR^(rev)/-*, eclosed without a visible bristle phenotype. A total of 7% of *BicDR^(rev)/-* animals contained an additional aSC bristle. Flies with the genotypes *BicDR⁷¹/-*, *EF1 γ ^{A70}/-*, and *EF1 γ ^{A51}/-* showed shorter pSC macrochaetae. Additionally, 21% of *BicDR⁷¹/-* animals eclosed with an extra aSC bristle, a similar frequency as observed with the alleles *EF1 γ ^{A42}/-* and *EF1 γ ^{A28}/-*. (I-K) Effect of combining heterozygous *EF1 γ ^{A70}*, *EF1 γ ^{A42}*, or *EF1 γ ^{A28}* with heterozygous *BicD* and *BicDR* alleles shows strong genetic interactions between heterozygous *BicD*, *BicDR*, and *EF1 γ* alleles. Frequency of mutant phenotypes observed in double and triple heterozygous combinations. Different mutant combinations containing a *BicDR**, *BicD^{PA66}*, and *EF1 γ ** allele eclosed with different bristle phenotypes. The frequency of animals that eclosed with a short-bristle phenotype is significantly higher if the animals carry a *BicD^{PA66}* and *BicDR⁷¹* allele except for the combination with *EF1 γ ^{A70}* where the frequency of flies with short bristles was the highest in *BicD^{PA66}/+; EF1 γ ^{A70}/+* (30%). Noticeable is that 19% of the flies with the genotype *BicD^{PA66}/+; BicDR⁷¹/EF1 γ ^{A28}* eclosed with short bristles, even though the allele *EF1 γ ^{A28}/-* induces additional bristles.

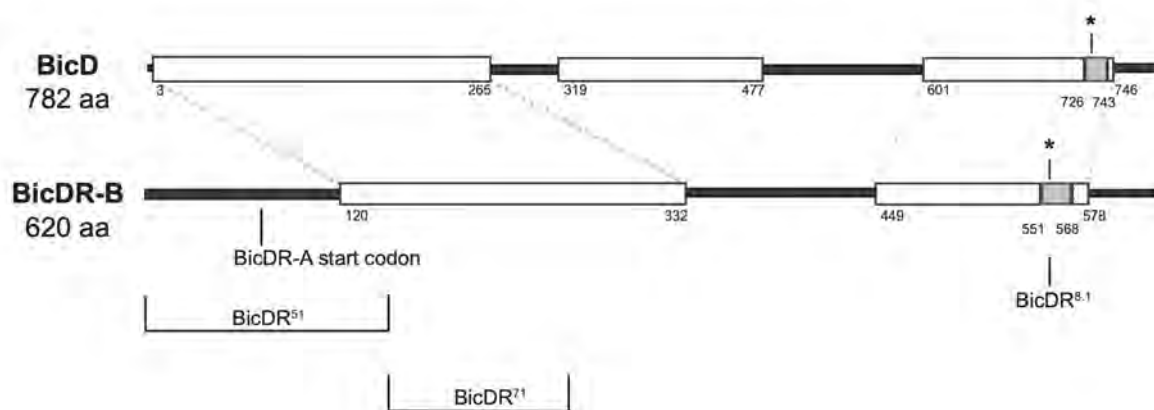
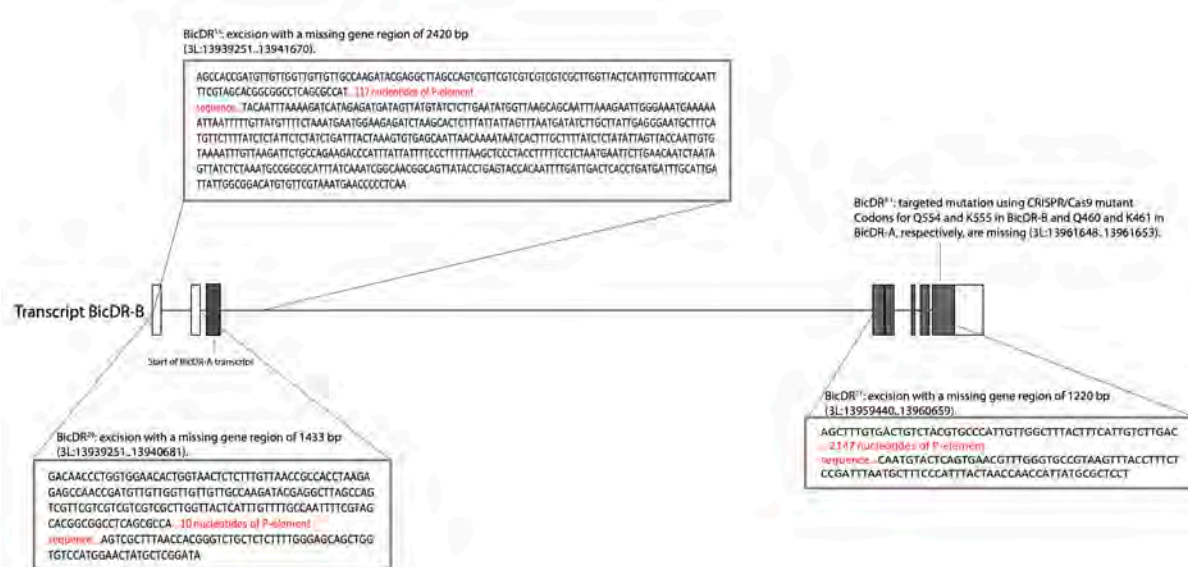
A**B**

Fig. S1. Comparing BicD and BicDR structures and the *BicDR* gene **A)** Structure comparison of the *Drosophila* proteins BicD and BicDR. Shown in open boxes are the coiled coil domains, in filled boxes the sequence with the highest homology. The lysine with a key role in cargo attachment is indicated with a star. It is localized at position 730 in BicD, at position 555 in BicDR-B, and 461 in BicDR-A. The regions altered in the different alleles are indicated. The hemizygous deletion *BicDR*^{8.1} removes precisely the two codons Q554 and K555 in *BicDR*. **B)** Structure of *Drosophila* *BicDR*-A and -B mRNAs and the excision mutants. The gray boxes frame the parts of the gene that have been removed by the imprecise P-element excisions. The sequences in the box show the position of the excision breakpoints. Sequences in red are P-element leftovers. The excision *BicDR*²⁹ misses the 5' UTR region, without impairing the first protein-coding exon, while *BicDR*⁵¹ misses the first protein coding exon of *BicDR*-A and -B and the 5' UTR region as well. *BicDR*⁷¹ is the only excision that removes protein coding exons 2, 3, and 4 but leaves exons 5 and 6 intact. *BicDR*^{8.1} is a CRISPR mutant with deleted Q554 and K555 codons.

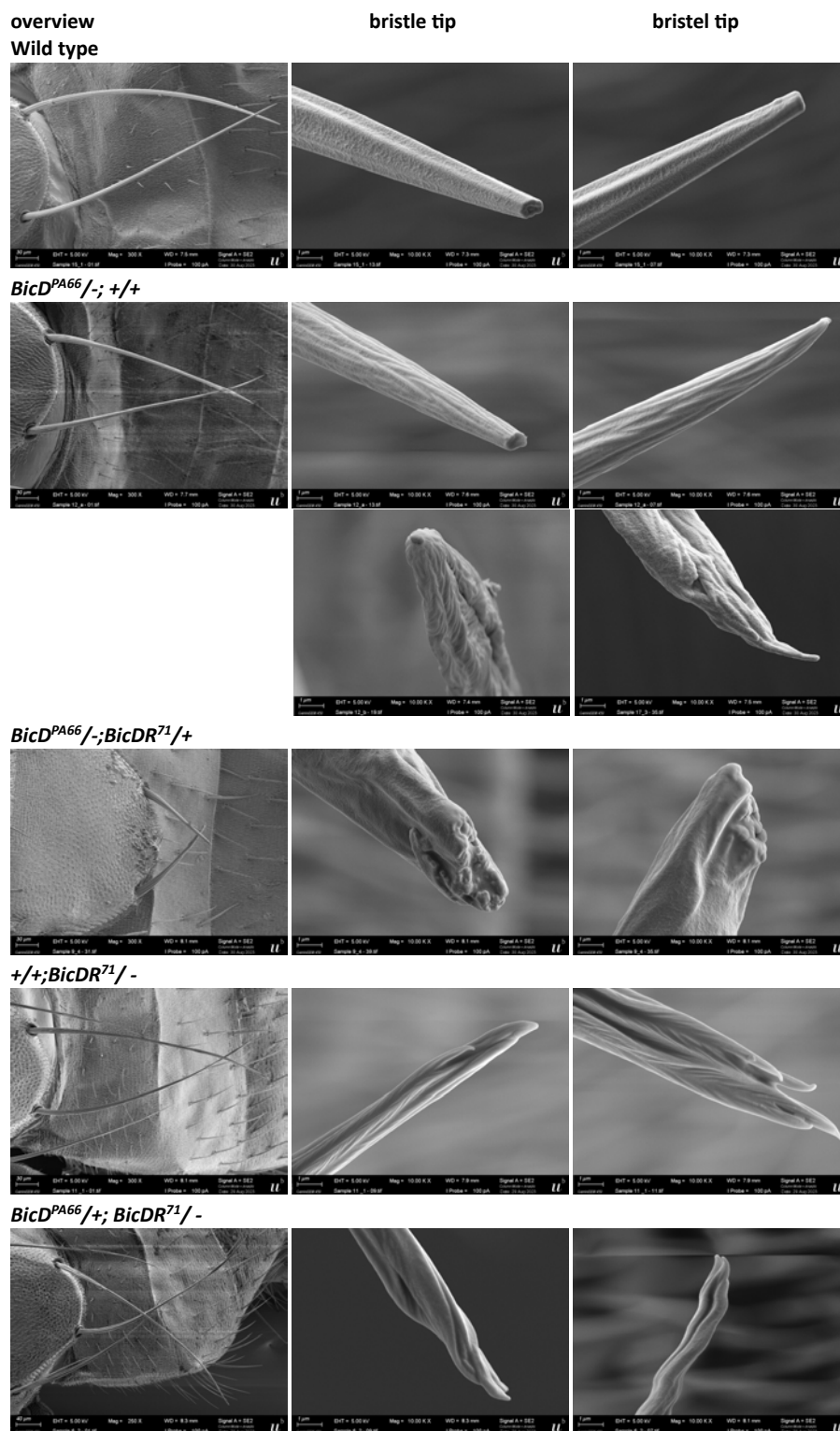


Fig. S2. Posterior scutellar bristles (pSC): overview (left) and corresponding bristle tips. The genotypes are indicated above the overview and the corresponding tips to the right. The 2nd chromosomes with the *BicD* gene and the 3rd with the *BicDR* gene are indicated. *BicD* alleles were *BicD*^{PA66} (PA66) and Df7068 (-). *BicDR* alleles were *BicDR*⁷¹ and Df4515 (-). “+” indicates a wild-type allele of *BicD* or *BicDR* either on an uncharacterized chromosome or a balancer chromosome. Additional examples from these and other *BicDR* alleles are shown in the *Supplementary data file S3*.

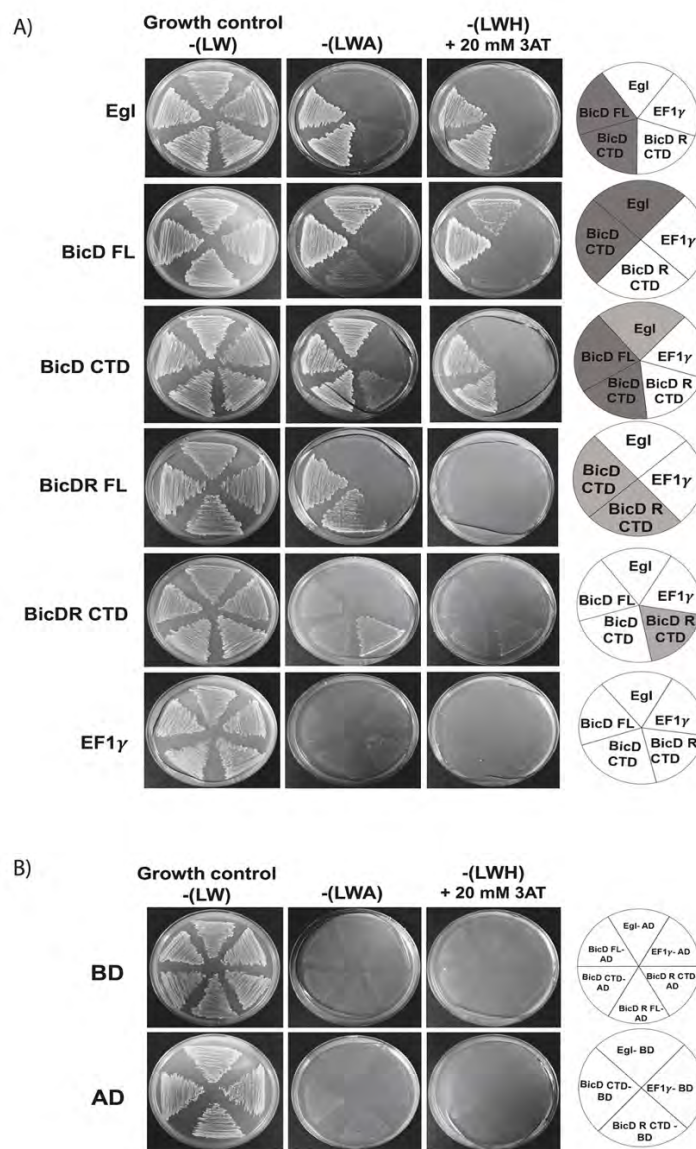
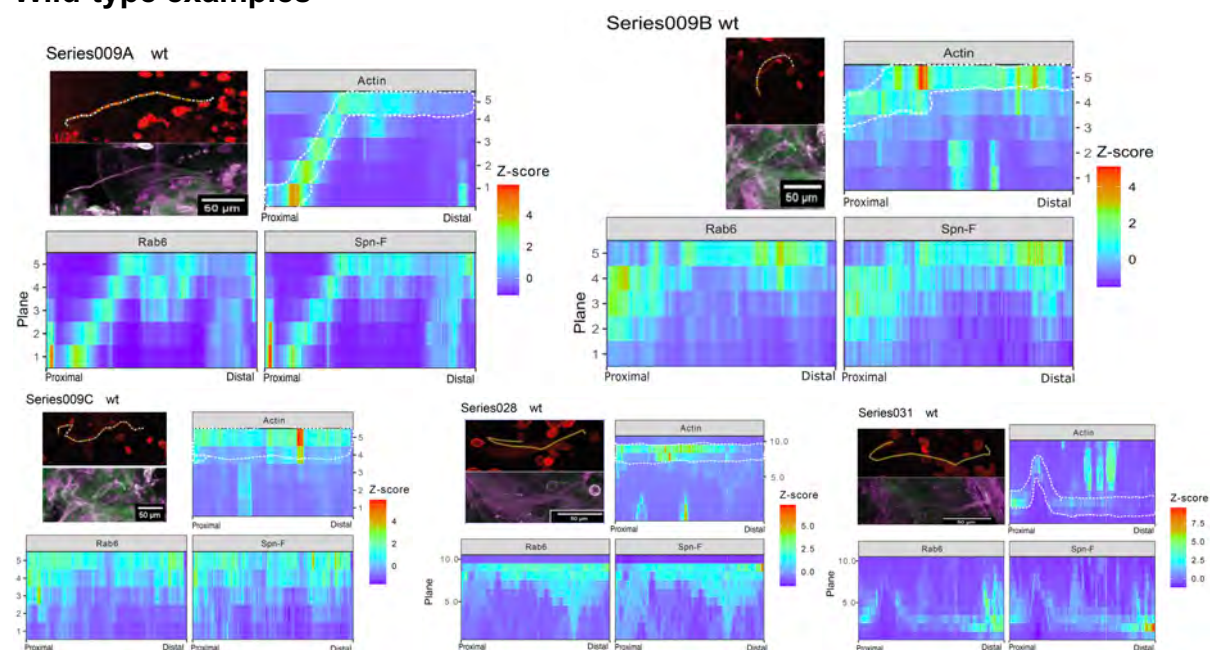
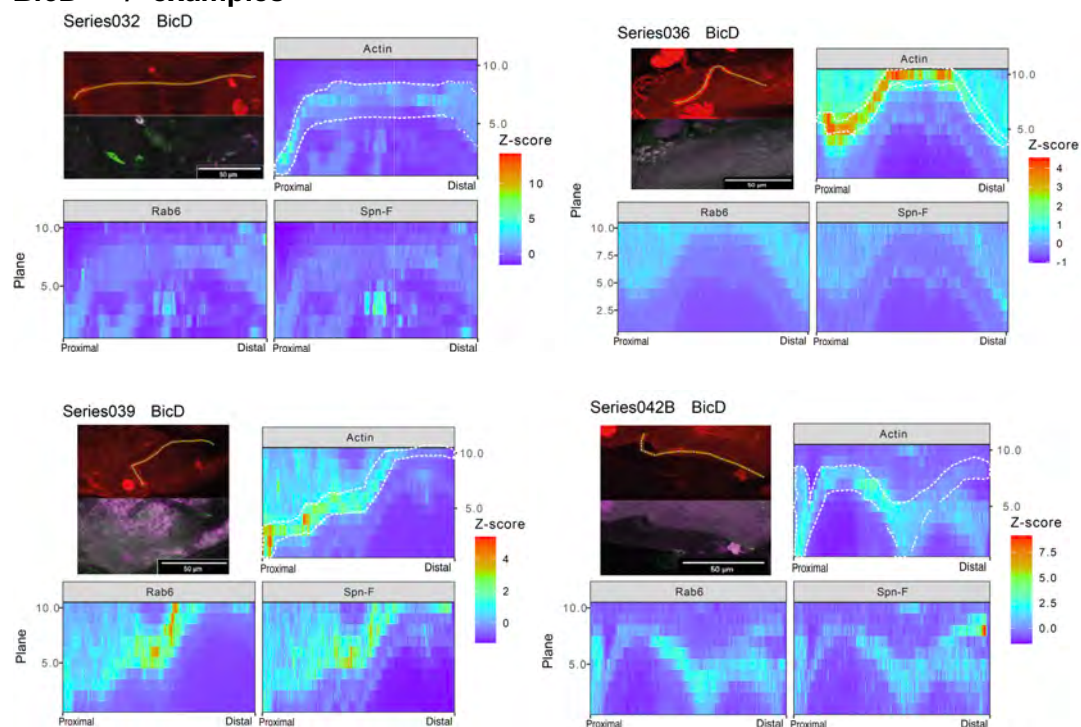


Fig. S3. *Drosophila* BicDR does not interact with EF1 γ , Egl, or BicD. (A) The activation domain is indicated on the left and the binding domains are on the right side. The latter is drawn where these activation domains were plated out. (-(LW): grown on medium selecting for the two plasmids, (-(LWH): selective plates on which cells with the activator domain and the DNA binding domain clones can grow if they weakly interact. (-(LWH) with 20 mM 3-aminotriazole [3-AT]: selective plates on which cells with the activator domain and the DNA binding domain clones can grow if they strongly interact. FL: full length, CTD: C-terminal domain, BD: binding domain, AD: activation domain. BicD and Egl were used as positive controls since their interaction had already been demonstrated⁷⁹. Here, the full-length protein of BicDR, fused to the activation domain, binds to the C-terminal domain of BicDR as well as to the C-terminal domain of BicD. However, this result is not confirmed under stringent conditions, since neither the full-length BicD protein nor the C-terminal domain of BicD seems to bind to BicDR in immunoprecipitations nor according to the yeast 2-hybrid assay. Thus, these results seem to indicate that the direct interaction between BicDR FL (AD) and BicD (BD) resulted from the nonspecific entanglement of the coiled coil domains⁸⁰. **(B)** Negative controls.

Wild-type examples



BicD^{PA66/-} examples



***BicD*^{PA66}/-; *BicDR*⁷¹/+ examples**

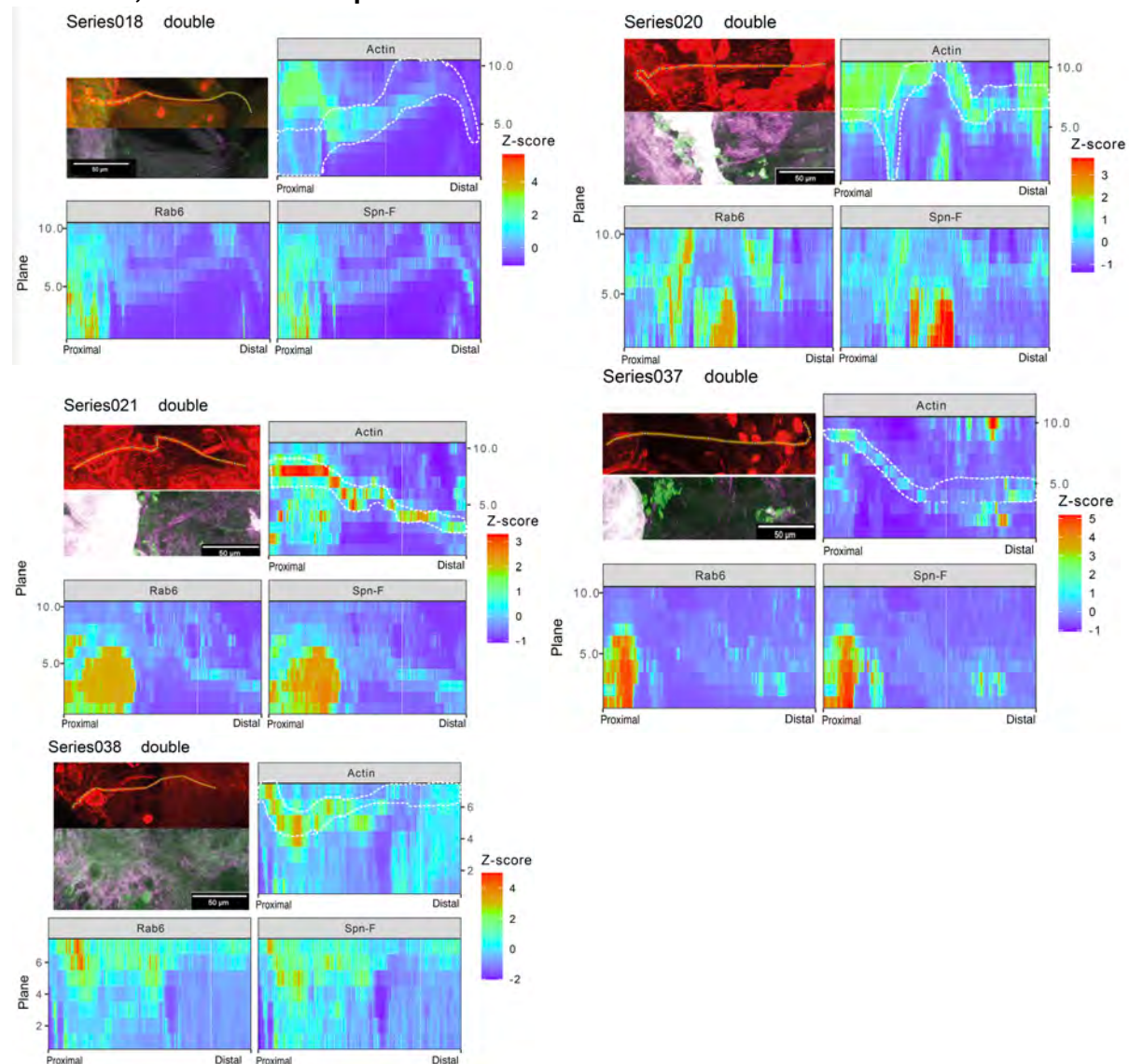
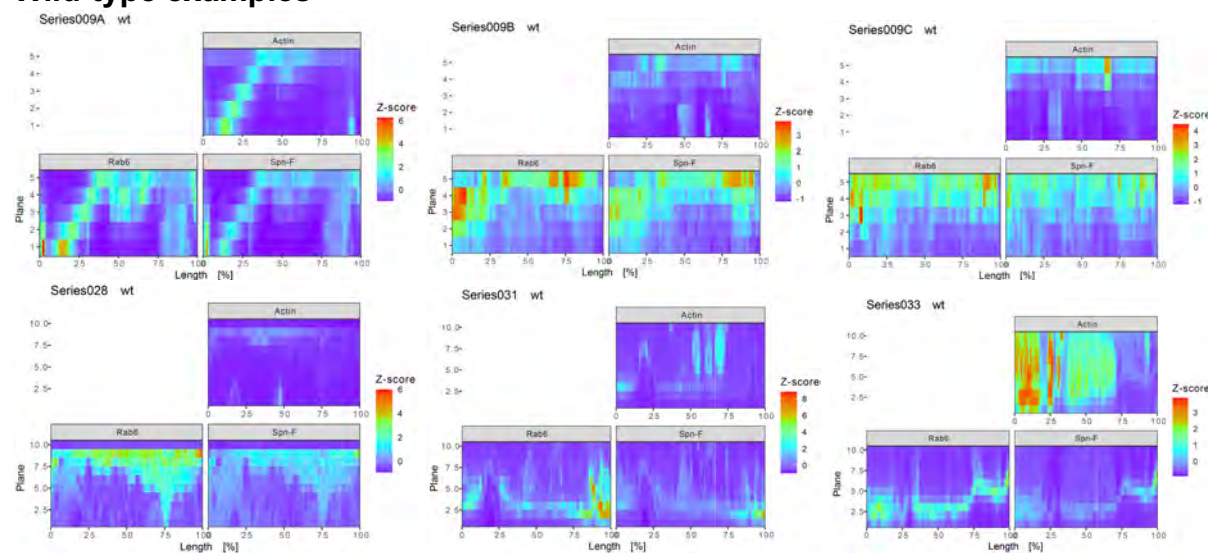


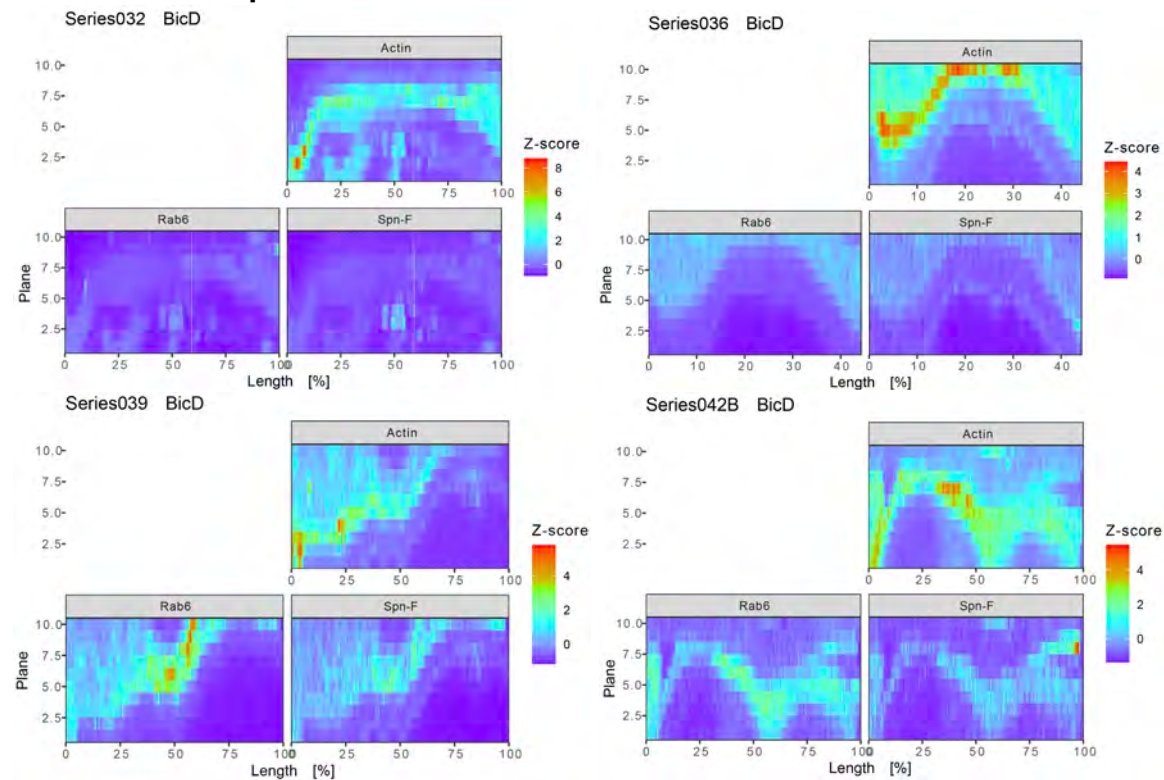
Fig. S4 (Display of signal intensity is normalized for each channel). This shows the distribution of the indicated signals; but levels cannot be compared between channels.

The top left picture shows a maximal projection of the region with the pupal posterior Scutellar Bristle (pSC). On top, the F-actin signal and a drawing of the line along which the staining intensities of the three channels were measured. Below, the staining for Spn-F in green and Rab6 in red. Pictures are oriented such that the proximal end of the bristle shaft is to the left side and the distal one to the right. The other three panels show the intensity of the signal in the different z-planes along the drawn line. The approximate position of the bristle shaft was estimated from the F-actin (Actin) and the Spn-F signal and is shown with a dashed line in the F-actin panel. The methods are described in the main part of the paper.

Wild-type examples



BicD^{PA66/-} examples



***BicD^{PA66}/-; BicDR⁷¹/+* examples**

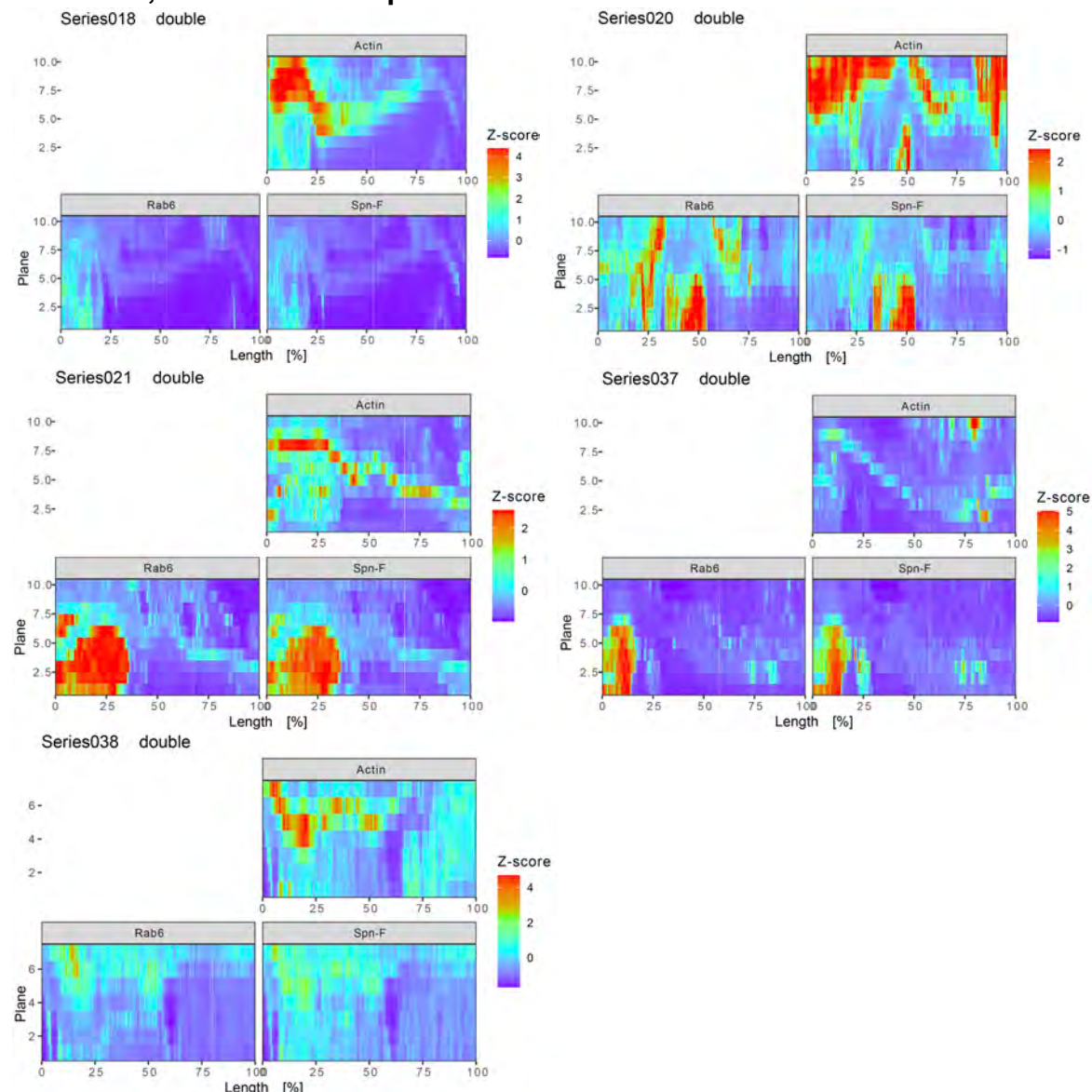


Fig. S5. Same data as in Figure S4 but with signal intensities normalized over the 3 channels. Taking the background signals into consideration, this allows to compare Rab6 and Spn-F expression levels along the bristle shaft across genotypes relative to F-actin. The maximal projection image and the approximate outline of the pSC through the z-stack planes are depicted in the corresponding top panels of Figure S4. Graphs are oriented such that the proximal end of the bristle shaft is to the left and the distal one to the right. The three panels show the intensity of the signal in the different z-planes measured along the pupal bristle (see Figure S4). The methods are described in the main part of the paper.

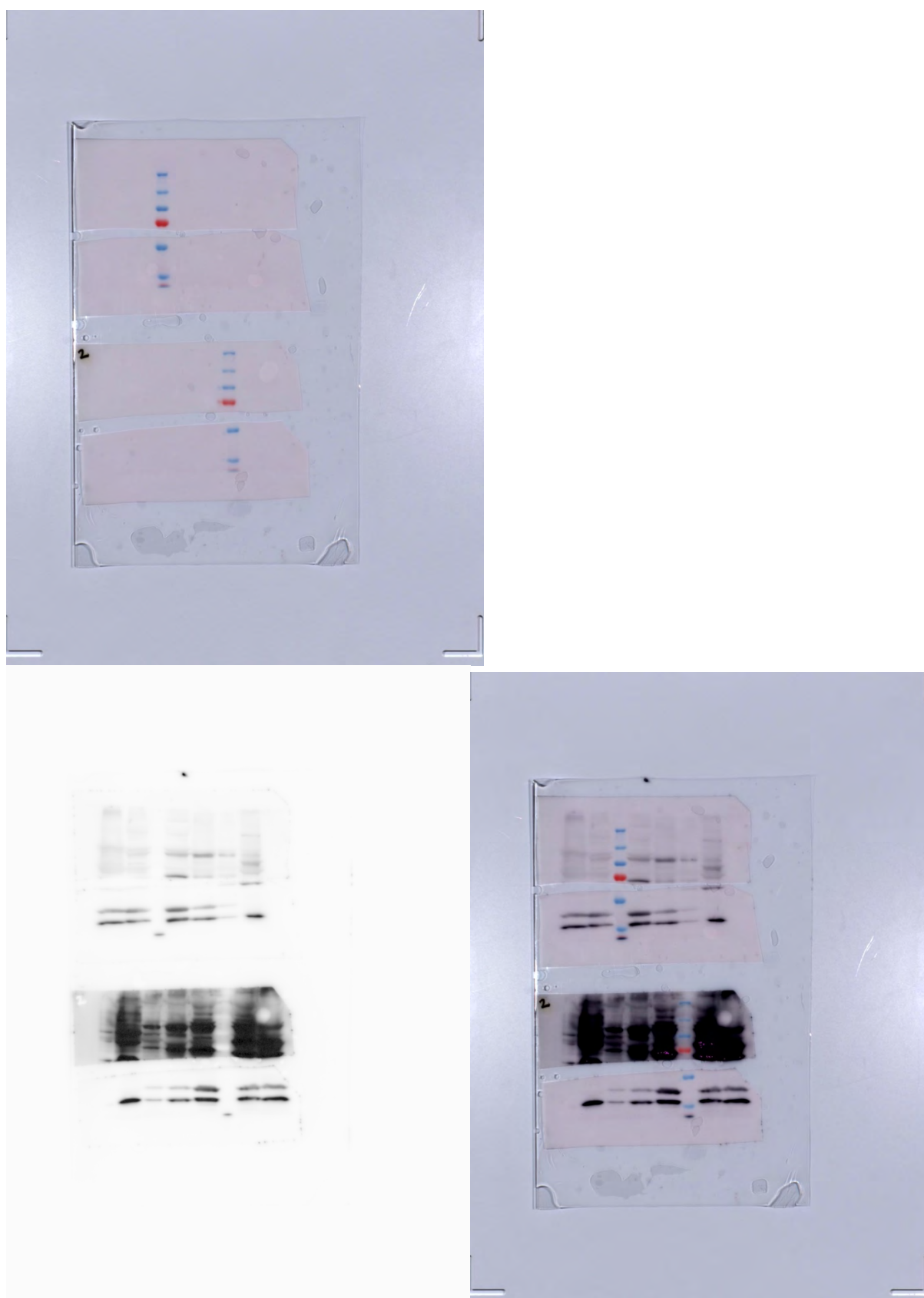


Fig. S6. Blot transparency

Table S1. Proteins that were significantly enriched in the tagged BicDR::GFP IPs in comparison to the wild-type negative control IPs. Genes encoding these proteins are listed according to their level of significance of enrichment over the control. The abbreviations used are “control” for the *white* control, “BicDR” (BicDR::GFP), and “BicDR^{K>A}” (BicDR^{K555A}::GFP). Hits enriched in tagged wild-type BicDR compared to BicDR^{K>A} are listed as potential cargo, whereas peptides enriched in tagged wild-type BicDR and BicDR^{K555A} IPs are listed as potential non-cargo interactors. GN is the abbreviation for gene name. The iBAQ equals the sum of all peptide intensities divided by the number of observable peptides of a protein¹. log₂FC is the logarithm of the mean ratio between the two groups and the adjusted p-value (adj. pVal) highlights the factor level comparisons within a family that are significantly different^{2,3}. -1 and -2: indicate different biological replicates.

GN	Sequence coverage [%]	iBAQ	log ₂ FC BicDR - control	log ₂ FC BicDR ^{K>A} - control	log ₂ FC BicDR ^{K>A} - BicDR	Adj. pVal BicDR - control	Adj. pVal BicDR ^{K>A} - control	Adj. pVal BicDR ^{K>A} - BicDR	Pot. Cargo	Pot. Non-cargo interactor
BicDR	84.7	1.70E+09	11.401	11.470	0.069	0.000	0.000	0.998	-	-
Phk-3	21.5	8.34E+06	3.745	3.478	-0.267	0.000	0.002	0.998		Yes
Dmel\CG10211	2.9	3.08E+05	3.546	4.039	0.493	0.000	0.000	0.998		Yes
Hsp67Bc	23.6	2.29E+06	3.513	4.133	0.620	0.002	0.002	0.998		Yes
Rac1	12.5	3.32E+06	3.039	1.662	-1.377	0.001	0.300	0.998	Yes	
BicDR::GFP	59.9	1.85E+07	2.804	3.021	0.217	0.002	0.024	0.998	-	-
I(2)k01209	4.6	1.11E+06	2.670	0.707	-1.963	0.015	0.774	0.998	Yes	
Kri	15.3	1.25E+07	2.242	1.486	-0.756	0.017	0.103	0.998	Yes	
Rp55a	49.6	2.85E+08	2.181	1.771	-0.410	0.024	0.099	0.998	Yes	
tou	1.8	2.80E+05	2.015	-0.341	-2.357	0.004	0.880	0.998	Yes	
Mtl	10.8	1.03E+07	1.796	1.192	-0.604	0.047	0.121	0.998	Yes	
mey	8.0	4.32E+06	1.741	0.498	-1.243	0.005	0.648	0.998	Yes	
Srp54k	35.0	2.57E+07	1.706	1.563	-0.143	0.004	0.024	0.998		Yes
Rp54	63.2	2.97E+08	1.689	1.373	-0.317	0.004	0.076	0.998	Yes	
RpL12	52.1	5.18E+08	1.680	1.538	-0.142	0.047	0.103	0.998	Yes	
Rp55b	43.5	1.11E+09	1.529	1.406	-0.123	0.013	0.036	0.998		Yes
RpS19a	96.2	3.66E+09	1.366	1.288	-0.078	0.047	0.100	0.998	Yes	
RpL27A	53.7	1.30E+08	1.315	1.234	-0.081	0.021	0.100	0.998	Yes	
RpS17	84.0	1.53E+09	1.290	1.210	-0.079	0.016	0.103	0.998	Yes	
RpL35	35.0	2.15E+08	1.289	0.872	-0.417	0.047	0.196	0.998	Yes	
Gp93	18.2	1.07E+07	1.273	0.688	-0.585	0.021	0.316	0.998	Yes	
RpL13	62.8	5.56E+08	1.143	0.826	-0.317	0.047	0.205	0.998	Yes	
RpL31	79.8	3.79E+08	1.104	0.915	-0.189	0.047	0.121	0.998	Yes	
RpS18	73.7	1.42E+09	1.095	0.983	-0.112	0.047	0.112	0.998	Yes	

Table S2. Out of the 118 proteins identified in the SDS-PAGE bands of BicDR::GFP immunoprecipitations, 21 are known to result in bristle phenotypes if perturbed. Abbreviations for BicDR::GFP: BicDR and BicDR^{K555A}::GFP: BicDR^{K>A}. The Sum PSM describes the summarized number of peptide spectrum matches of the sample with the indicated genotype. Primary data is from Supplementary Data file S2.

Description	Percent Coverage	Protein length	Sum PSM BicDR_1	Sum PSM BicDR_2	Sum PSM BicDR ^{K>A} _1	Sum PSM BicDR ^{K>A} _2	Reference for bristle phenotype
B52	7.6	355	1	3	0	0	4
RpS3A	12.6	246	0	3	0	0	5
Cpb	10.9	276	0	4	0	0	6
RpS17	19.1	131	0	2	0	0	7
Arp3	31.6	418	10	3	0	0	8
RpS3A	40.7	268	9	15	0	0	9
Orc6	23.0	257	2	5	0	0	10
RE01362p (Fragment)	30.0	299	0	14	0	0	11
Orc4	16.3	459	6	1	0	0	12
Vha26	52.2	226	22	18	0	0	13
Rumi	5.7	316	1	0	0	0	14
Par-6	29.6	351	7	1	0	0	15
Ef1y	52.0	431	80	43	6	0	16
NAT1	5.6	1488	0	1	3	4	17
Arm	2.0	843	5	4	1	0	18
Parvin	12.0	367	3	1	2	0	19
CtBP	10.3	476	0	2	0	1	20
Hrb27C	27.3	421	17	14	1	0	17
Hsp83	2.9	717	4	4	2	0	21
Sam-S	24.0	408	0	7	1	0	22
Arp2	22.8	399	0	9	2	2	23

References for Tables S1-2

1. Fabre, B. *et al.* Comparison of label-free quantification methods for the determination of protein complexes subunits stoichiometry. *EuPA Open Proteomics* **4**, 82–86 (2014).
2. Wright, S. P. Adjusted P-Values for Simultaneous Inference. *Biometrics* **48**, 1005 (1992).
3. Wang, M. *et al.* Amino acid metabolism, lipid metabolism, and oxidative stress are associated with post-stroke depression: A metabonomics study. *BMC Neurol.* **20**, 1–10 (2020).

4. Kraus, M. E. & Lis, J. T. The concentration of B52, an essential splicing factor and regulator of splice site choice in vitro, is critical for *Drosophila* development. *Mol. Cell. Biol.* **14**, 5360–5370 (1994).
5. Sæbøe-Larssen, S., Lyamouri, M., Merriam, J., Oksvold, M. P. & Lambertsson, A. Ribosomal Protein Insufficiency and the Minute Syndrome in *Drosophila*: A Dose-Response Relationship. *Genetics* **148**, 1215–1224 (1998).
6. Hopmann, R. & Miller, K. G. A balance of capping protein and profilin functions is required to regulate actin polymerization in *Drosophila* bristle. *Mol. Biol. Cell* **14**, 118–128 (2003).
7. Hart, K., Klein, T. & Wilcox, M. A Minute encoding a ribosomal protein enhances wing morphogenesis mutants. *Mech. Dev.* **43**, 101–110 (1993).
8. Rajan, A., Tien, A. C., Haueter, C. M., Schulze, K. L. & Bellen, H. J. The Arp2/3 complex and WASp are required for apical trafficking of Delta into microvilli during cell fate specification of sensory organ precursors. *Nat. Cell Biol.* **11**, 815–824 (2009).
9. Casad, M. E. *et al.* Cardiomyopathy is associated with ribosomal protein gene haplo-insufficiency in *Drosophila melanogaster*. *Genetics* **189**, 861–870 (2011).
10. Balasov, M., Akhmetova, K. & Chesnokov, I. Humanized *drosophila* model of the Meier-Gorlin syndrome reveals conserved and divergent features of the Orc6 protein. *Genetics* **216**, 995–1007 (2020).
11. Zielke, N., Vähärautio, A., Liu, J., Kivioja, T. & Taipale, J. Upregulation of ribosome biogenesis via canonical E-boxes is required for Myc-driven proliferation. *Dev. Cell* **57**, 1024–1036.e5 (2022).
12. McDaniel, S. L. *et al.* Tissue-Specific DNA replication defects in *drosophila melanogaster* caused by a meier-gorlin syndrome mutation in *orc4*. *Genetics* **214**, 355–367 (2020).
13. Le Bras, S., Rondanino, C., Kriegel-Taki, G., raldine, Dussert, A. & Borgne, R. Le. Genetic identification of intracellular trafficking regulators involved in Notch-dependent binary cell fate acquisition following asymmetric cell division. *J. Cell Sci.* **125**, 4886–4901 (2012).
14. Acar, M. *et al.* Rumi Is a CAP10 Domain Glycosyltransferase that Modifies Notch and Is Required for Notch Signaling. *Cell* **132**, 247–258 (2008).
15. Besson, C. *et al.* Planar cell polarity breaks the symmetry of PAR protein distribution prior to mitosis in *Drosophila* sensory organ precursor cells. *Curr. Biol.* **25**, 1104–1110 (2015).
16. Fan, Y. *et al.* *Drosophila* Translational Elongation Factor-1 γ Is Modified in Response to DOA Kinase Activity and Is Essential for Cellular Viability. *Genetics* **184**, 141–154 (2010).
17. Mummery-Widmer, J. L. *et al.* Genome-wide analysis of Notch signalling in *Drosophila* by transgenic RNAi. *Nature* **458**, 987–992 (2009).
18. Lin, X. & Perrimon, N. Dally cooperates with *Drosophila* Frizzled 2 to transduce Wingless signalling. *Nature* **400**, 281–284 (1999).
19. Chountala, M., Vakaloglou, K. M. & Zervas, C. G. Parvin Overexpression Uncovers Tissue-Specific Genetic Pathways and Disrupts F-Actin to Induce Apoptosis in the Developing Epithelia in *Drosophila*. *PLoS One* **7**, (2012).
20. Stern, M. D. *et al.* CtBP is required for proper development of peripheral nervous system in *Drosophila*. *Mech. Dev.* **126**, 68–79 (2009).

21. Milton, C. C., Batterham, P., McKenzie, J. A. & Hoffmann, A. A. Effect of E(sev) and Su(Raf) Hsp83 mutants and trans-heterozygotes on bristle trait means and variation in *Drosophila melanogaster*. *Genetics* **171**, 119–130 (2005).
22. Larsson, J. & Rasmuson-Lestander, Å. Somatic and germline clone analysis in mutants of the S-adenosylmethionine synthetase encoding gene in *Drosophila melanogaster*. *FEBS Lett.* **427**, 119–123 (1998).
23. Koch, N. *et al.* Abp1 utilizes the Arp2/3 complex activator Scar/WAVE in bristle development. *J. Cell Sci.* **125**, 3578–3589 (2012).

Table S3. Publicly available fly stocks used in this thesis.

BL stands for “Bloomington Stock Center” and VDRC for “Vienna RNAi Center”.

Name	ID
37870	VDRC# 37870
32137R 2 III	VDRC# 32137R 2 III
Df(3L)ED4515	BL# 9071
Df(3L)BSC737	BL# 26835
Df(2L)Exel7068	BL# 7838
nos-Cas9	BL# 54591
nos-phiC31 int	BL# 25709
eEF1gamma[A42]	BL# 40962
eEF1gamma[A70]	BL# 40963
eEF1gamma[A28]	BL# 40964
eEF1gamma[A15]	BL# 40965
Df(3R)Exel6212	BL# 7690

Table S4. Primers used in this study.

The primers listed in this table were used for the generation of *BicDR::GFP* and *BicDR^{K555A}::GFP* expressing flies and for the yeast 2-hybrid experiment. as described in the methods section.

Name	Sequence	Application
<i>BicDR</i> homologous Arm 1 fwd	5'- atcgtcgGCGGCCGCTCTAAATGGATTCTAACTAACC-3'	Generation of <i>BicDR::GFP</i> expressing flies
<i>BicDR</i> homologous Arm1 rvs	5'- ACTTCCGGATCCTGCTCGTGAAATAAACTC-3'	Generation of <i>BicDR::GFP</i> expressing flies
GFP primer 1 fwd	5'- CGAGCAGGATCCGGAAGTGGATCTATGGTGAGCAAGGGCGAG-3'	Generation of <i>BicDR::GFP</i> expressing flies
GFP primer 1 rvs	5'- CTCCAAGAATTCTTACTTGTACAGCTCGTCCA-3'	Generation of <i>BicDR::GFP</i> expressing flies
<i>BicDR</i> homologous Arm 2 fwd	5'- AAGTAAGAATCTTGAGTAACCTAACGACCCGCTGG-3'	Generation of <i>BicDR::GFP</i> expressing flies
<i>BicDR</i> homologous Arm 2 rvs	5'- cgacgatGGGCCCCGACGTGGACAATAATGA-3'	Generation of <i>BicDR::GFP</i> expressing flies
Mutagenesis Primer for BicDRK555A fwd	5'- GCAAGCGGTCGAGCTGTAC-3'	Generation of <i>BicDR^{K555A}::GFP</i> expressing flies
Mutagenesis Primer for BicDRK555A rvs	5'- GTGACAGCTCGACCGCTTGC-3'	Generation of <i>BicDR^{K555A}::GFP</i> expressing flies
Screening fwd	5'- CCACATGAAGCAGCACGAC-3'	Generation of <i>BicDR::GFP</i> and <i>BicDR^{K555A}::GFP</i> expressing flies
Screening rvs	5'- CTACGAACAGAAGAAGGGCA-3'	Generation of <i>BicDR::GFP</i> and <i>BicDR^{K555A}::GFP</i> expressing flies
BicDR-full -Sense	5'- accaccatggcaattccccgggATGCATAAACCAAGCTAGCGAA -3'	Yeast 2-Hybrid experiment
BicDR-full -Anti	5'- gcaggtcgacggatccccgggTTATCGCTGAAATAAACTCCAAAGC -3'	Yeast 2-Hybrid experiment
BicDR-CTD sense	5'- accaccatggcaattccccgggAGTTTGCAATTCGAAATGGAATG -3'	Yeast 2-Hybrid experiment
BicDR-CTD rvs	5'- gcaggtcgacggatccccgggTTATCGCTGAAATAAACTCCAAAGC -3'	Yeast 2-Hybrid experiment
eIF1gamma sense	5'- accaccatggcaattccccgggATGGTGAAAGGAACTCTGTACACTTACC -3'	Yeast 2-Hybrid experiment
eIF1gamma Anti	5'- gcaggtcgacggatccccgggTACTTGAAGATCTTGCCCTGGT -3'	Yeast 2-Hybrid experiment